NASA CR 134507

A THERMAL, THERMOELASTIC, AND WEAR ANALYSIS OF HIGH-ENERGY DISK BRAKES

F.E. KENNEDY, J.J. WU, AND F.F. LING

TRIBOLOGY LABORATORY
MECHANICS DIVISION
RENSSELAER POLYTECHNIC INSTITUTE
TROY, NEW YORK 12181

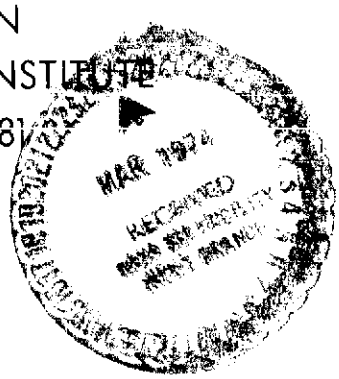

January 1974

Prepared for

AEROSPACE SAFETY RESEARCH AND DATA INSTITUTE
LEWIS RESEARCH CENTER
NATIONAL AERONAUTICS AND SPACE ADMINISTRATION
CLEVELAND, OHIO 44135

UNDER

NASA GRANT NGR 33-018-152

S. WEISS, TECHNICAL MONITOR

R.L. JOHNSON, TECHNICAL ADVISOR

1. Report No.	2. Government Accession No.	3. Recipient's Catalog No.
NASA CR 134507		

4. Title and Subtitle	5. Report Date
A Thermal, Thermoelastic, and Wear Analysis of High-Energy Disk Brakes	January 1974
	6. Performing Organization Code
7. Author(s)	8. Performing Organization Report No.
F.E. Kennedy, J.J. Wu and F.F. Ling	
	10. Work Unit No.
9. Performing Organization Name and Address	11. Contract or Grant No.
Rensselaer Polytechnic Institute Troy, New York 12181	NGR 33-018-152
	13. Type of Report and Period Covered
12. Sponsoring Agency Name and Address	Contractor Report
National Aeronautics and Space Administration Washington, D.C. 20546	14. Sponsoring Agency Code

15. Supplementary Notes

Sponsored by Aerospace Safety Research and Data Institute Lewis Research Center
C. David Miller - Technical Monitor
R.L. Johnson - Technical Advisor

16. Abstract

This report describes a thermomechanical investigation of the sliding contact problem encountered in high-energy disk brakes. The analysis includes a modelling, using the finite element method of the thermoelastic instabilities that cause transient changes in contact area to occur on the friction surface. In order to include the effect of wear at the contact surface, a wear criterion is proposed that results in the prediction of wear rates for disk brakes that are quite close to experimentally determined wear rates. The thermal analysis shows that the transient temperature distribution in a disk brake assembly can be determined more accurately by use of this thermomechanical analysis than by a more conventional analysis that assumes constant contact conditions. It also shows that lower, more desirable, temperatures in disk brakes can be attained by increasing the volume, the thermal conductivity, and, especially, the heat capacity of the brake components.

17. Key Words (Suggested by Author(s))	18. Distribution Statement
Surface temperature Friction and wear Finite element method	Unclassified - unlimited

19. Security Classif. (of this report)	20. Security Classif. (of this page)	21. No. of Pages	22. Price*
Unclassified	Unclassified	~~59~~ 54	$5.75

* For sale by the National Technical Information Service, Springfield, Virginia 22151

NASA-C-168 (Rev. 6-71)

FOREWORD

This work was conducted as part of NASA Grant NGR 33-018-152 from the Office of University Affairs, Washington, D. C. 20546. Mr. C. David Miller of NASA's Aerospace Safety Research and Data Institute was the technical monitor. Mr. R. L. Johnson, Manager of NASA's Lubrication Research Branch was the technical advisor. Dr. F. F. Ling, Chairman of RPI's Mechanics Division was the principal investigator. Acknowledgement is made of the many helpful suggestions made by C. David Miller and R. L. Johnson of NASA during the course of this investigation, and of Mr. S. Weiss who is the new technical monitor.

TABLE OF CONTENTS

SECTION 1

SUMMARY

This report describes a thermomechanical investigation of the sliding contact problem encountered in high-energy disk brakes. The analysis includes a modelling, using the finite element method of the thermoelastic instabilities that cause transient changes in contact area to occur on the friction surface. In order to include the effect of wear at the contact surface, a wear criterion is proposed that results in the prediction of wear rates for disk brakes that are quite close to experimentally determined wear rates. The thermal analysis shows that the transient temperature distribution in a disk brake assembly can be determined more accurately by use of this thermomechanical analysis than by a more conventional analysis that assumes constant contact conditions. It also shows that lower, more desirable, temperatures in disk brakes can be attained by increasing the volume, the thermal conductivity, and, especially, the heat capacity of the brake components.

SECTION 2

INTRODUCTION

This thermal and thermoelastic investigation will consider the sliding contact problem encountered in high-energy disk brakes of the type used in the wheels of large aircraft. In such brakes large amounts of thermal energy are generated at the friction surfaces and this can cause very high temperatures and large thermal deformation in the brake components, overheating of the wheel components, excessive wear of the contacting surfaces, and, possibly, unsatisfactory braking performance. An accurate knowledge of the temperature distribution and thermal deformation in these high-energy brakes, especially near the sliding interfaces, is necessary in order to insure that the brakes will perform reliably under the severe conditions encountered in service.

The thermal analysis of bodies in sliding contact has attracted the interest of many investigators because of its importance in many situations in which friction occurs. Most work has been concerned with relatively light loading situations, for which experiments have shown that contact occurs mainly at and near surface asperities, with localized high "flash temperatures" occurring at the small contact spots. Most analyses of this type of temperature distribution have assumed that the contact spots are widely-separated and do not interact, thus enabling application of a solution for the case of a single isolated contact based on the work of Blok (Ref.1) and/or Jaeger (Ref.2). A different approach for this situation has been to assume a stochastic model for heat generation which considers the distribution of the spots of actual contact on the friction surface to be random in both space and time (Ref.3,4).

Although these investigations have given much useful information about temperatures occurring in low-energy sliding systems, they cannot completely describe the situation in brakes, where the loading is relatively severe. Several experimental investigations (Ref.5,6,7) have shown that when large loads are applied to sliding bodies the contact areas are not small and widely-separated like asperities, but are discrete areas that are intermediate between asperity size and the dimensions of the apparent contact area.

Barber (Ref.6) has shown graphically that the formation and movement of these areas of actual contact are determined by the thermomechanical processes of thermal deformation and wear. A non-uniform pressure distribution on the contact surface causes non-uniform heat generation, with higher temperatures resulting at areas of greatest contact. Greater thermal expansion at the hot contact areas causes contact to become more concentrated at those areas until wear is great enough to force the contact to shift elsewhere. Thus, "thermo-elastic instability" occurs on the contact surface. Although Barber assumed that the initial non-uniformity arose because of surface irregularities, other analyses (Ref.8,9) have shown that even for smooth surfaces the heat generated at the sliding interface can cause changes in pressure distribution and contact area.

It is apparent from the above discussion that an accurate analysis of transient temperatures in high-energy sliding systems must account for thermal deformation, and vice versa. Previous brake analyses have neglected this inter-dependence, and have assumed that either the entire contact area (Ref.10) or widely-separated spots (Ref.11,12) remained in contact throughout the braking period. In our work a thermomechanical analysis will be performed, using the finite element method, in which the contact areas and the pressure distribution within them will be determined by a thermoelastic analysis and will then be used in a thermal analysis to find the transient temperature distribution in the disk brake. A wear model will be proposed that will allow both the modeling of the thermoelastic instabilities observed by Barber and the estimation of the amount of wear that occurs on the contact surface. The effect of different material parameters on the temperature distribution will be investigated in an attempt to determine the parameters most important for safe and reliable brake performance. No analysis of this type has yet been reported and it is felt that it would be difficult, if not impossible, to carry out the analysis using classical techniques.

SECTION 3

METHOD OF ANALYSIS

3.1 The Physical Problem and its Finite Element Idealization

A typical aircraft disk brake assembly is shown in Figure 1a. The brake consists of a number of stationary and rotating disks, with the rotating disks being splined to the aircraft wheel. When the brake is applied, a hydraulic piston exerts pressure on the end disks and this pressure is transmitted through the stack, causing friction between the stator and rotor disks and transforming large amounts of kinetic energy to thermal energy.

In our analysis of the temperature distribution and thermal deformation in the disk brake we will examine a typical section shown in Figure 1b. The section is bounded by plane A-A, the midplane of a stator disk, and plane B-B, the midplane of a rotor disk, and contains one friction surface. We will assume that the midplanes of the stator and rotor disks are planes of symmetry for both deformation and temperature fields. It will also be assumed that the total force acting on planes A-A and B-B is the same as that applied to the end disks by the hydraulic piston, thus neglecting friction at the splines. The rotating disk usually consists of a segmented lining, often of hardened alloy steel, attached to a thin annular disk. A typical stator disk consists of a number of pads containing friction material rigidly attached to both sides of an annular backplate. In our work we will assume that variations in temperature, stress, and displacement in the circumferential direction can be neglected in both stator and rotor, thus enabling an axisymmetric analysis.

The finite element idealization to be used in this analysis is shown in Figure 2a. The geometry of the model has been chosen to conform as closely as possible to that of an actual aircraft wheel brake. Except for those calculations in which the effect of different material parameters is being studied, all material properties used in the investigation will be the properties of the actual brake materials. Letters A through E are assigned to points inside the brake that are referred to in later sections of this report.

The finite elements used in the analysis will be axisymmetric ring elements of triangular cross-section. At the friction surface, however, a slight variation will be made. It is quite important that effects of directional stiffness in those

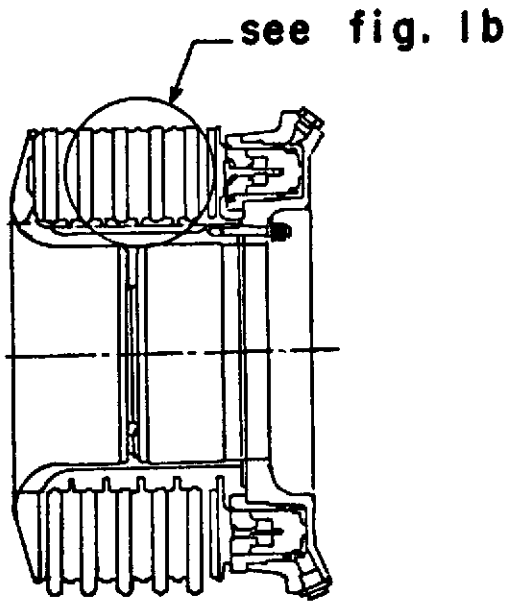

Figure 1a. Profile of Typical Aircraft Brake

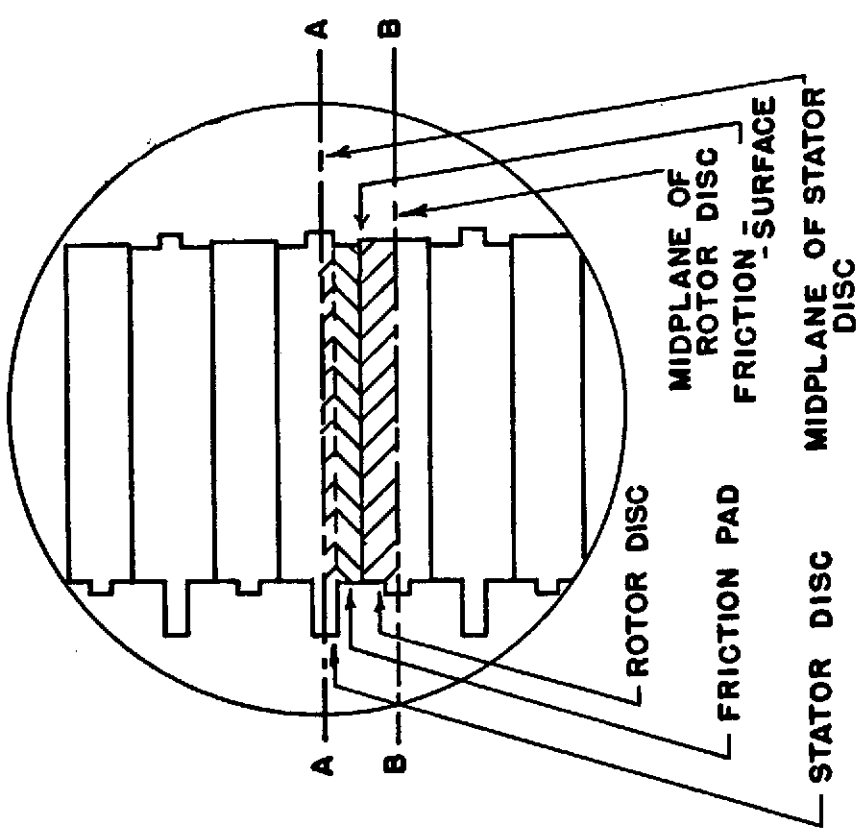

Figure 1b. Section of the Rotor-Stator Stack

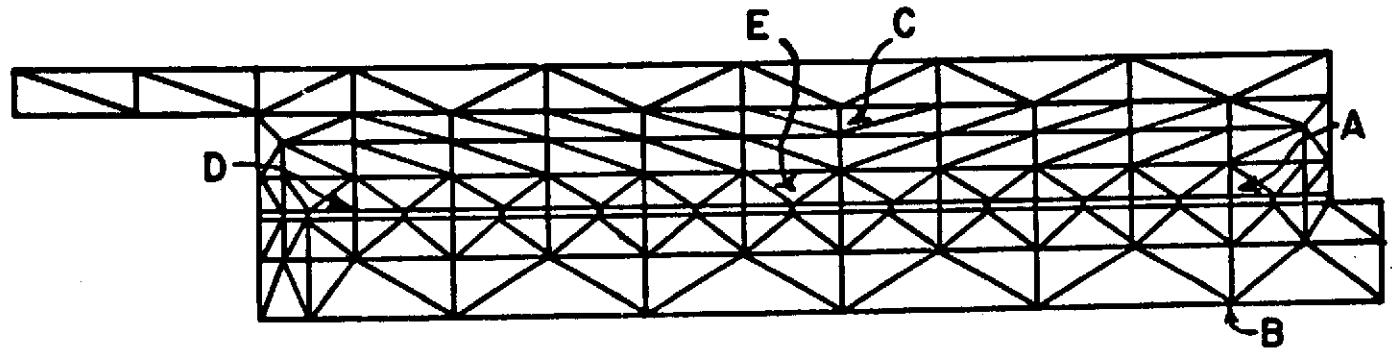

Figure 2a. Finite Element Idealization of Brake Section

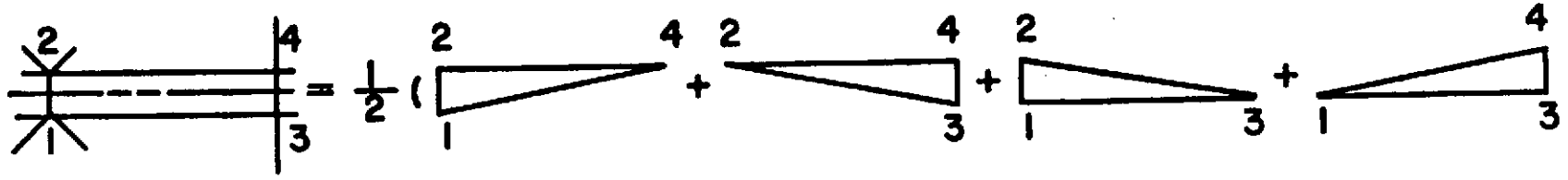

Figure 2b. A Typical Source Element. Element nodes identified by numbers 1 - 4.

elements be eliminated as much as possible since it is those elements in which contact occurs, heat is generated, and wear is possible. In order to accomplish this a new composite element has been developed for the friction surface by superposition of four triangular ring elements. In this superposition, which is shown in Figure 2b, each set of two triangular elements consists of one surface element from the stator disk and one from the rotor, with each element having one-half of its normal stiffness. The result is a quadrilateral composite element which is composed of both stator and rotor materials. We will call these elements "source elements" and will discuss in later sections their part in heat generation, wear analysis, and contact area determination.

The procedures to be developed here for analysis of an annular disk brake will also be applied to a similar analysis of a caliper disk brake, so that the analytical results can be compared with experimental data obtained recently (Ref.7) for that type of brake. The caliper brake, which is similar to the disk brakes used in automobiles, is not actually axisymmetric, but will be approximated as such for the purposes of this analysis.

A difference in the finite element idealization for the single pad problem is that the elements in the stationary disk (the pad) are no longer rings, but are now ring sectors. The composite source elements for this configuration are made up of two rotor elements of volume $2\pi\bar{r}A$ and two pad elements of volume $\beta\bar{r}A$, where A is the cross-sectional area of the triangular elements, $\bar{r}$ is the centroidal radius of the element, and β is the included angle of the ring sector.

In all our work we will assume that coupling between the thermal and thermoelastic equations can be neglected, so that the two equations may be analyzed separately.

3.2 Procedure for Thermal Analysis

Our analysis of the temperature distribution in the brake will be carried out using the finite element method, which has been applied to the investigation of heat conduction problems by a number of analysts in the past seven or eight years.

It can be shown (see Appendix A) that the set of nodal temperatures $\{T_i\}$ in a body obeying Fourier's law of heat conduction may be found for a given set of

boundary conditions by solving a matrix equation of the form:

$$[TS]\{T_i\} = \{FT\} \tag{1}$$

where [TS] is a "thermal stiffness matrix" dependent on the thermal properties of the body and {FT} is the matrix of "thermal loads" applied to the body, consisting of heat generation, prescribed heat flux, and convection at the boundary. Equation (1) is the basic finite element equation to be used in our thermal analysis. The formation of the matrices to be used in Eq.(1) and the solution of that matrix equation is, for the most part, straightforward. The boundary conditions and the heat generation at the friction surface require further explanation, however.

For our work we will assume that the mechanical work done by friction is entirely transformed into heat energy and that this heat is generated inside the source elements on both sides of the friction surface. This is in line with the conclusion by Ling and Pu (Ref.3) that the heat is generated slightly below the friction surface by means of material deformation.

Before each incremental thermal analysis a thermoelastic analysis must be performed (see following sections) and from that analysis we will know which source elements are in contact at the beginning of the increment and the stresses in those contacting elements. Since the friction surface lies in the center of the source elements, the pressure P_e acting on the friction surface will be the σ_z acting at the centroid of the source element. It will be assumed that this pressure and the contact area remain constant throughout the time increment and that short time increments will be specified so that this assumption will be reasonably valid.

If the angular deceleration $\dot{\omega}$ of the wheel remains constant during the braking cycle, the heat generation rate in the source element during a time increment of length Δt will be:

$$\dot{Q} = \frac{P_e f \bar{r} A_p}{J} \left[\Omega - \dot{\omega}\left(t - \frac{\Delta t}{2}\right)\right] \tag{2}$$

where

A_p = contacting area of stator element $= \frac{\beta}{2}(r_o^2 - r_i^2)$

f = coefficient of friction

$\bar{r}, r_o, r_i$ = centroidal, outside, and inside radii of element

Ω = initial angular velocity of wheel

t = time at end of increment

J = conversion constant between mechanical work and heat energy.

The source elements are made up of four triangular elements of thickness h_e, with two of the elements being in the stator (friction pads) with contacting area A_p, and two in the rotating disk with contacting area $A_D = \pi(r_o^2 - r_i^2)$. If the heat generation rate/unit volume in each of the triangular elements is $\dot{q}$, then

$$\dot{q} = \frac{P_e f \bar{r} A_p}{J h_e (A_p + A_D)} \left[\Omega - \dot{\omega}\left(t - \frac{\Delta t}{2}\right)\right] \tag{3}$$

for source elements that are in contact. For all other elements $\dot{q} = 0$. (Note: for annular brake $A_p = A_D$.)

A partitioning of the generated heat between pad and disk elements is not necessary in our finite element analysis, since the heat, once generated, may easily be conducted across the friction surface. The thermal resistance due to the formation of oxide films on the friction surface (Ref.22) will be neglected here.

In our investigation, since all heat input is taken care of by the above generation terms, there will be no non-zero prescribed heat flux $\vec{q}^o$, on any surface. Since midplanes A-A and B-B (see Fig.1b) are planes of symmetry for the temperature field, there will be no heat flux across those planes. Although no heat flux will be prescribed on the inner and outer boundaries of the section, heat transfer by convection at those surfaces could be allowed in cases where brake cooling is being considered.

3.3 Procedure for Thermoelastic Stress Analysis

The loading on our brake section consists of both axisymmetric and antisymmetric loads. Both the pressure applied at the midplanes of the disks and the temperature field are axisymmetric and the stresses and deformation caused by them will be found using the axisymmetric finite element equations for uncoupled thermoelasticity.

The additional loading caused by friction at the contact surface is antisymmetric, and the stresses resulting from this loading will be added to the axisymmetric stresses by superposition. In the source elements, which are the only

elements for which a stress distribution is required, the sole antisymmetric contribution to the stress field is:

$$\tau_{z\theta} = fP_e \qquad (4)$$

where P_e is the axisymmetric stress component σ_z acting at the center of the source element.

The finite element equation that will be employed in the axisymmetric stress analysis is of the well-known form

$$[ST]\{DIS\} = \{FN\} = \{F_T\} + \{F_F\} + \{F_S\} + \{P\} \qquad (5)$$

where [ST] is the system stiffness matrix, {DIS} is the matrix of nodal displacements, and {FN} is the matrix of nodal loads, with the latter being made up of contributions from thermal stresses, body forces, surface tractions, and concentrated external forces. The details of the derivation of (5) may be found elsewhere (Ref.14,15), but briefly the derivation proceeds as follows: A potential energy functional π^e is determined that is valid in each element of the elastic body. An appropriate function, in our case linear, is used to relate the value of the independent displacements at a point inside an element to their values at the element nodes, and this function is used, along with the stress-strain and strain-displacement relations of linear elasticity, to get the potential energy functional π^e in terms of nodal displacements. The first variation of the elemental potential energy functional, $\delta\pi^e$, is then found with respect to admissible variations in nodal displacements and, after summing the $\delta\pi^e$ for all elements, the principle of minimum potential energy, $\Sigma\delta\pi^e = 0$, is applied to get the resulting equation (5). It might be noted that (5) is similar in form to Eq.(1), the finite element equation for use in the thermal analysis, thus enabling use of the same computer subroutines for the solution of both equations.

For the axisymmetric analysis we will use the following boundary conditions on the external boundary: (referring to Fig.1b)

on midplane B-B $\quad w = 0$ (fixed for reference purposes)

$\tau_{rz} = 0$

on midplane A-A $\quad w = \delta$ (constant with respect to r)

$\tau_{rz} = 0.$

With these boundary conditions the midplanes remain plane and symmetry is preserved. We will also assume that all surface tractions on the inside and outside boundaries are zero, and that bending stresses may be neglected.

The value of δ will be such that at all times the total applied load is F_{appl}, the force applied by the hydraulic piston. We will assume that this applied force, but not necessarily the pressure distribution caused by it, remains constant throughout the braking cycle. In order to determine the δ that will produce a total applied force of F_{appl} during an increment we proceed as follows:

For each time increment we will assume a displacement $w = \delta$ on midplane A-A, solve matrix equation (5) for the displacements {DIS}, and use these displacements to find the stresses present in each element. The elastic stresses will then be integrated numerically along a plane parallel to A-A and the resultant F_{tot} in the direction perpendicular to A-A will be compared with the given applied load F_{appl}. If $F_{tot} \neq F_{appl}$ a correction will be made to δ such that the equality will exist after the displacements and stresses are recomputed.

After we have found a solution for the incremental stress distribution for which $F_{tot} = F_{appl}$, we may proceed to determine whether any changes in contact area have occurred in the increment.

3.4 Contact Area Determination

Transient changes in actual contact area occur on both the microscopic (surface asperity) and macroscopic scale during sliding contact between deformable bodies. In our work we will examine only the macroscopic changes and will assume that within areas of gross contact the number of asperity contacts is large enough that perfect contact is attained. Similarly, within the areas of non-contact it will be assumed that the number of asperity contacts is so small that no effective contact occurs.

In our contact area determination we will examine each source element individually, after having calculated the thermoelastic stress distribution using the methods of the previous section. Changes in contact area will therefore occur by means of the addition or subtraction of the bands of contact swept out by single source elements. For our finite element mesh, the single element bands will each comprise less than 5% of the total possible contact area. The contact/non-contact determination for the individual elements will proceed as follows:

For elements presently in contact:

The criterion for contact is $P_e < 0$ (compression), where P_e is the value of σ_z at the center of the source element. If the criterion is met, the element remains in contact through the next iteration. If, however, $P_e > 0$, a tensile stress is present at the contact surface and that is impossible. In order to remove the element from contact and to make the resulting adjustments in the stress field, we will use the stress transfer method, which was originally developed for a "no-tension" rock mechanics application (Ref.16).

The non-contacting source elements will, in effect, contain a fissure and will be unable to sustain any normal and shear stresses on the contact surface. Those elements become, therefore, transversely isotropic, with the stress-strain constitutive relationship being given by

$$\{\sigma'\} = \begin{Bmatrix} \sigma'_r \\ \sigma'_\theta \\ 0 \\ 0 \end{Bmatrix} = \frac{E}{(1+\nu)(1-2\nu)} \begin{bmatrix} 1-\nu & \nu & 0 & 0 \\ \nu & 1-\nu & 0 & 0 \\ 0 & 0 & 0 & 0 \\ 0 & 0 & 0 & 0 \end{bmatrix} \begin{Bmatrix} \epsilon_r \\ \epsilon_\theta \\ \epsilon_z \\ \epsilon_{rz} \end{Bmatrix} = [D']\{\epsilon\} \qquad (6)$$

For the same elastic strain $\{\epsilon\}$, however, our finite element analysis, which assumes isotropic material behavior, predicts an elastic stress

$$\{\sigma_e\} = \begin{Bmatrix} \sigma_r \\ \sigma_\theta \\ \sigma_z \\ \tau_{rz} \end{Bmatrix} = \frac{E}{(1+\nu)(1-2\nu)} \begin{bmatrix} 1-\nu & \nu & \nu & 0 \\ \nu & 1-\nu & \nu & 0 \\ \nu & \nu & 1-\nu & 0 \\ 0 & 0 & 0 & \frac{1-2\nu}{2} \end{bmatrix} \begin{Bmatrix} \epsilon_r \\ \epsilon_\theta \\ \epsilon_z \\ \epsilon_{rz} \end{Bmatrix} = [D]\{\epsilon\} \qquad (7)$$

The excess stress $\{\Delta\sigma''\} = \{\sigma_e\} - \{\sigma'\}$ must be transferred from the source element to surrounding elements and this is done by equilibrating $\{\Delta\sigma''\}$ by a set of forces $\{P''\}$ acting on the element nodes and then removing the set of forces to allow the body to deform further. Although in most stress transfer applications the system stiffness matrix [ST] is left unchanged and a number of stress transfer iterations are done until $\{\sigma_e\} = \{\sigma'\}$, it has been found advantageous in this analysis to recompute [ST] using the constitutive relation given in (6) for all non-contacting source elements. This enables a large reduction in the number of stress transfer iterations required.

In addition to the inability of the non-contacting source elements to transmit loads across the fissured contact surface, they also are unable to conduct heat across the interface. This is accomplished in our analysis by setting $k_z = 0$ in the thin source elements which are no longer in contact. This necessitates a change in the thermal stiffness matrix [TS] at the same time that [ST] is recomputed. Because of these stiffness matrix changes, the non-contact elements will have $\sigma_z = \tau_{rz} = \tau_{z\theta} = 0$, $k_z = 0$, and $\dot{q} = 0$ until the stiffness matrices are changed again when the elements come back into contact.

For source elements presently not in contact:

In addition to examining the contacting elements to see if contact has been lost, we must also examine non-contacting source elements to see if contact has resumed at those elements. The stress in the elements not in contact will be given by (6), while the axisymmetric stress that would be present if the element were in contact is given by (7). If σ_{ze} at the center of the element is compressive ($P_e < 0$) then the element has resumed contact and the stress transfer process must be used again, this time to transfer stress back to the element. In this case the stress to be transferred is $\{\Delta\sigma''\} = \{\sigma'\} - \{\sigma_e\}$.

We will also have to change [ST] and [TS] again, this time returning the element's contributions to their original values. After these changes have been accomplished and the stress has been transferred, the element can be treated like any other contacting source element.

3.5 Wear Analysis using the Stress Transfer Method

Although wear is one of the most common modes of material behavior, it is very difficult to express accurately a quantitative law for wear prediction because of the many factors that affect wear. A large amount of research in this area has been carried out in the past 20 years in an attempt to get a better understanding of the wear process and, although it has not resulted in a wear law that can be used in our work, a number of observations have been made which help us in our approximation of such a law (Ref.17,18,19). It is assumed that the following conclusions drawn from metallic wear research (Refs.17,18,19), will also hold true for all materials under investigation here.

- Wear rates are, in general, directly proportional to load, and inversely proportional to the hardness or yield stress of the material being worn.
- When two materials of different hardness are in sliding contact, wear is usually more severe in the softer material.
- Wear usually increases with increasing temperature. Although this is due to many factors, mainly metallurgical, it has been shown by Lancaster (Ref.20) that, at least for some materials under certain conditions, most of the increase of wear with temperature is accounted for by a decrease in hardness with increasing temperature.
- Wear is dependent more upon distortion or shear stresses than upon dilatational stresses. Analytical models for low wear have been developed which use the maximum shear stress as a measure of loading (Ref.21).

Based on these observations and upon the requirement that, for our incremental finite element analysis, wear should take place in discrete steps instead of by the actual continuous process, the following wear criterion was chosen for use here:

If the energy of distortion for a source element, given by the second invariant, J_2, of the stress deviator tensor, equals or exceeds a critical value, W, based on the temperature-dependent yield stress of the element material, wear will occur. If $J_2 < W$ no wear will occur in the element. For our analysis

$$J_2 = \frac{1}{6}\left[(\sigma_r - \sigma_\theta)^2 + (\sigma_\theta - \sigma_z)^2 + (\sigma_z - \sigma_r)^2 + 6\tau_{rz}^2 + 6\tau_{z\theta}^2\right] \tag{8}$$

and

$$W \equiv \frac{\sigma_y^2}{3}$$

where $\sigma_y = \sigma_y(T)$ for the softer of the two materials in the composite source element.

In order to prevent our wear criterion from being satisfied when the source element is not in contact, we will also require that the magnitude of $\tau_{z\theta}$ acting at the friction surface have a finite value, or $|\tau_{z\theta}| > 0$.

Upon examination of the above, it can be seen that our wear criterion is actually a modified criterion for plastic flow. Although the occurrence of wear in most materials is preceded by some localized plastic deformation, we will be neglecting the plastic deformation in our work. We will instead assume that,

when the distortional strain energy reaches the critical value at which yielding would normally occur, most of this energy is transformed into surface energy and a wear particle is formed. The removal of this particle requires the presence of a frictional force acting on the particle. Although this model is admittedly a simplification of the wear process, such simplification is necessary in order to quantitatively analyze this complicated phenomenon.

For our finite element idealization the source elements are the only ones in which wear can occur, but the source elements are made up of elements of both stator and rotor materials. Since wear will not usually occur in both materials at the same time, we must calculate W for both materials in a contacting source element and compare the smaller of the two values with J_2 for the element. If $J_2 > W$ for that softer material, the resulting wear will be assigned to the contacting surface of that material inside the element.

Once the wear criterion indicates that wear has occurred in an element, the magnitude of the wear and the post-wear stress and displacement distributions must be determined. To aid in this determination we will assume that when wear occurs in an element a thin layer of material is removed from the element at the friction surface. After removal of this material the element is allowed to expand at constant temperature in the z-direction only by an amount w_w such that, after the wear process, $\sigma_z = 0$ and $\tau_{rz} = 0$ at the friction surface.

The numerical procedure for carrying out the wear process will be the stress transfer method. If the axisymmetric stress matrix before wear is given by $\{\sigma_o\}$ and after wear by $\{\sigma'\}$, where

$$\{\sigma_o\} = \begin{Bmatrix} \sigma_r \\ \sigma_\theta \\ \sigma_z \\ \tau_{rz} \end{Bmatrix} \qquad \text{and} \qquad \{\sigma'\} = \begin{Bmatrix} \sigma'_r \\ \sigma'_\theta \\ 0 \\ 0 \end{Bmatrix}$$

then the stress that must be transferred from the element is

$$\{\Delta\sigma''\} = \{\sigma_o\} - \{\sigma'\}$$

where, since displacement occurs in the z-direction only,

$$\sigma_r - \sigma'_r = \sigma_\theta - \sigma'_\theta = \frac{\nu}{1-\nu}\,\sigma_z .$$

Upon carrying out the transfer of stress it will again be found advantageous to change the stiffness matrix of the element to that based on Eq.(6) and achieve rapid convergence using the new stiffness matrix.

If the elastic strain of the element after conclusion of the transfer process is given by $\{\epsilon\}$, then the total amount of stress relieved in the element by the wear process is

$$\{\sigma_w\} = ([D] - [D'])\{\epsilon\} \tag{9}$$

where $[D']$ is given by Eq.(6).

Since we have restricted displacement to the z-direction during the isothermal wear process, the strain occurring during wear is,

$$\{\epsilon_w\} = \begin{Bmatrix} 0 \\ 0 \\ \frac{\partial w}{\partial z} \\ \frac{\partial w}{\partial r} \end{Bmatrix} \tag{10}$$

We have chosen the displacements to be linear functions of the coordinates, so

$$\frac{\partial w}{\partial z} = \frac{w_w}{h_e} \tag{11}$$

where h_e is the element thickness (z-direction).

A relationship may now be found for the worn thickness w_w by using (10), (11), (7) and (9):

$$D_{13}\epsilon_r + D_{23}\epsilon_\theta + D_{33}\epsilon_z \equiv \sigma_{zz} = D_{33}\frac{w_w}{h_e}$$

or

$$w_w = \frac{\sigma_{zz} h_e}{D_{33}} \tag{12}$$

Knowing σ_{zz}, which is the z-component of the stress that would be present in the element if no wear had occurred, we can calculate the amount of wear that took place in the element. It should be noted that if wear has previously occurred in the element it must be taken into account when calculating σ_{zz}, so that we will have

$$\sigma_{zz} = D_{13}\epsilon_r + D_{23}\epsilon_\theta + D_{33}\epsilon_z - \Sigma\sigma_{w_z}$$

where the summation is taken over all previous wear occurrences in the element.

If a resumption or loss of contact occurs in a worn source element, it will be handled by the procedures developed in Section 3.3. The stress required for resumption of contact will be different from that given in Eq.(7), however, since for a worn element (9) becomes

$$\{\sigma_e\} = [D]\{\epsilon\} - \Sigma\{\sigma_w\} \tag{9a}$$

where the Σ is taken over all wear occurrences in the element.

It might be noted that because of the assumption of axisymmetry, wear in this analysis takes place in finite steps or delaminations during which an annular layer of material is removed. Although such annular strips are not normally found in wear debris, they can be considered to be made up of the many short flat wear particles that are usually observed.

A block diagram and flow chart showing the computational process used in the solution of this problem is included in Appendix B.

SECTION 4

RESULTS AND DISCUSSION

4.1 Analysis of Single-Pad Brake

The analytical procedures outlined in the past section will first be applied to a thermomechanical investigation of a caliper-type disk brake having one friction pad on each face of a rotating disk. Such a brake has recently been studied experimentally at the RPI Tribology Laboratory by Santini (Ref.7).

The finite element idealization will be similar to that shown in Figure 2 with the stator elements being ring sectors. The friction materials will be those used in the Boeing 747 aircraft brake, with the rotating disk being of high strength alloy steel and the friction pad composed of a sintered copper-based composite enclosed in a carbon steel cup. The stator backplate will be aluminum, and in order to account for the thermal contact resistance between it and the friction pad, several elements at that interface will be assigned zero conductivity perpendicular to the interface. Although some cooling of the rotating disk takes place in practice, it will be neglected here and all external surfaces will be assumed to be insulated.

We will assume that the friction pad and rotating disk both are initially relatively smooth and that, upon initial application of the brake, perfect contact occurs across the entire pad surface. Because of a difference in sliding velocity between inside and outside radii, however, the heat generation rate varies across the pad. This causes a nearly immediate concentration of the contact area to a region near the outside of the friction pad. This contact area change is illustrated in Figure 3 in which the complete initial contact is shown at the top ($\theta = 0$). Soon the contact becomes more and more concentrated in one small band near the outside of the pad. The stress level in the small contact area gets quite high and shortly (at $\theta \approx .25$) wear occurs at the concentrated contact and several other source elements come into contact. Once again a concentration of contact occurs, followed by wear and a shift of contact to another area, and this cycle repeats itself a great many times during brake application. Thermoelastic instabilities of the type experimentally observed by Barber (Ref.6) are therefore predicted by this disk brake analysis.

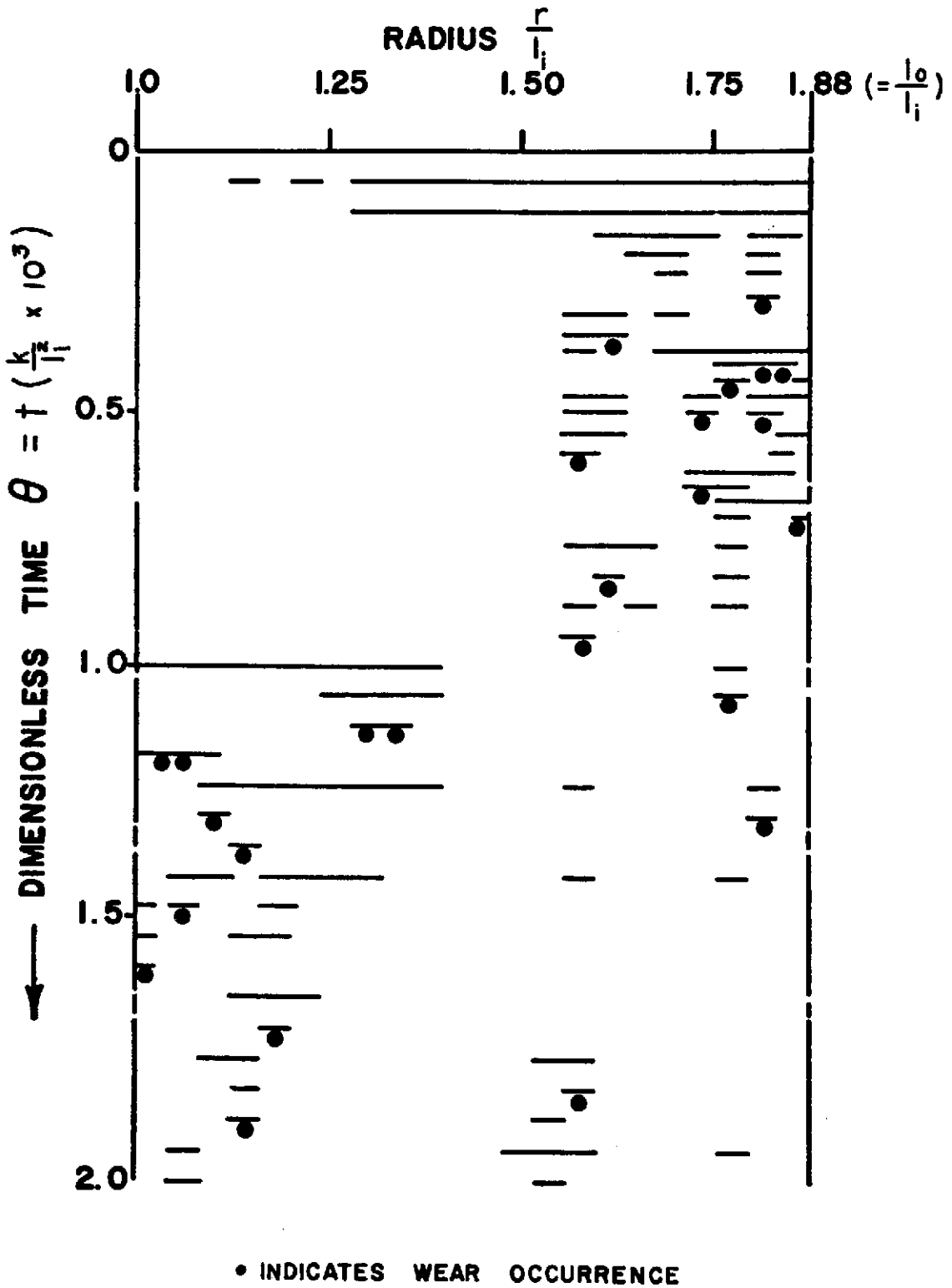

Figure 3. Transient Changes in Contact Area for Single-Pad Brake. Horizontal lines indicate portions of friction surface in contact.

At any one time the temperature distribution on the friction surface is very non-uniform, with temperatures being quite high in contact zones or zones that have just worn, and lower elsewhere. If uniform contact pressure had been maintained during braking, with no changes in contact area occurring, a non-uniform temperature distribution would still be predicted because of the non-uniform velocity distribution, but the degree of non-uniformity is much greater with the variable contact analysis.

Because of the changes in contact area, the temperature at each point on the friction surface fluctuates with time. In Figure 4 one can see the transient temperature curves for three points inside the friction pad near the contact surface. For each point the temperature determined by this analysis is compared with that found by experiment (Ref.7), and with that found by a constant-contact analysis. The latter analysis neglects the effect of thermoelastic deformation and was carried out using the same computer program, but setting $\alpha = 0$ for all materials. The three points investigated are points A, D, and E, as defined in Figure 2. The dimensionless temperature φ used for all curves is defined as

$$\varphi = \frac{Tk_1\bar{\ell}}{\dot{Q}_o} \times 10^3$$

where

k_1 = thermal conductivity of conventional friction pad material

$\bar{\ell}$ = average radius of friction pad

$\dot{Q}_o$ = initial rate of heat generation.

The upper set of curves in Figure 4 shows the temperature at point D, located near the inside radius of the pad surface, while the middle set of curves shows the temperature at point E near the center of the pad surface. The gradual temperature rise at point E throughout the period under investigation and at point D during early portions of the time period indicate that concentrated contact was not occurring near those points. Later, at about $\theta = 1.5$, both the experimental data and the thermoelastic analysis show a rise in temperature as contact starts occurring near point D (see also Fig.3). Although the thermoelastic analysis predicts greater fluctuation in transient temperature than does the experimental data, it is perhaps due to the fact that the experimental data is the average of a number of test runs, with fluctuations being averaged out.

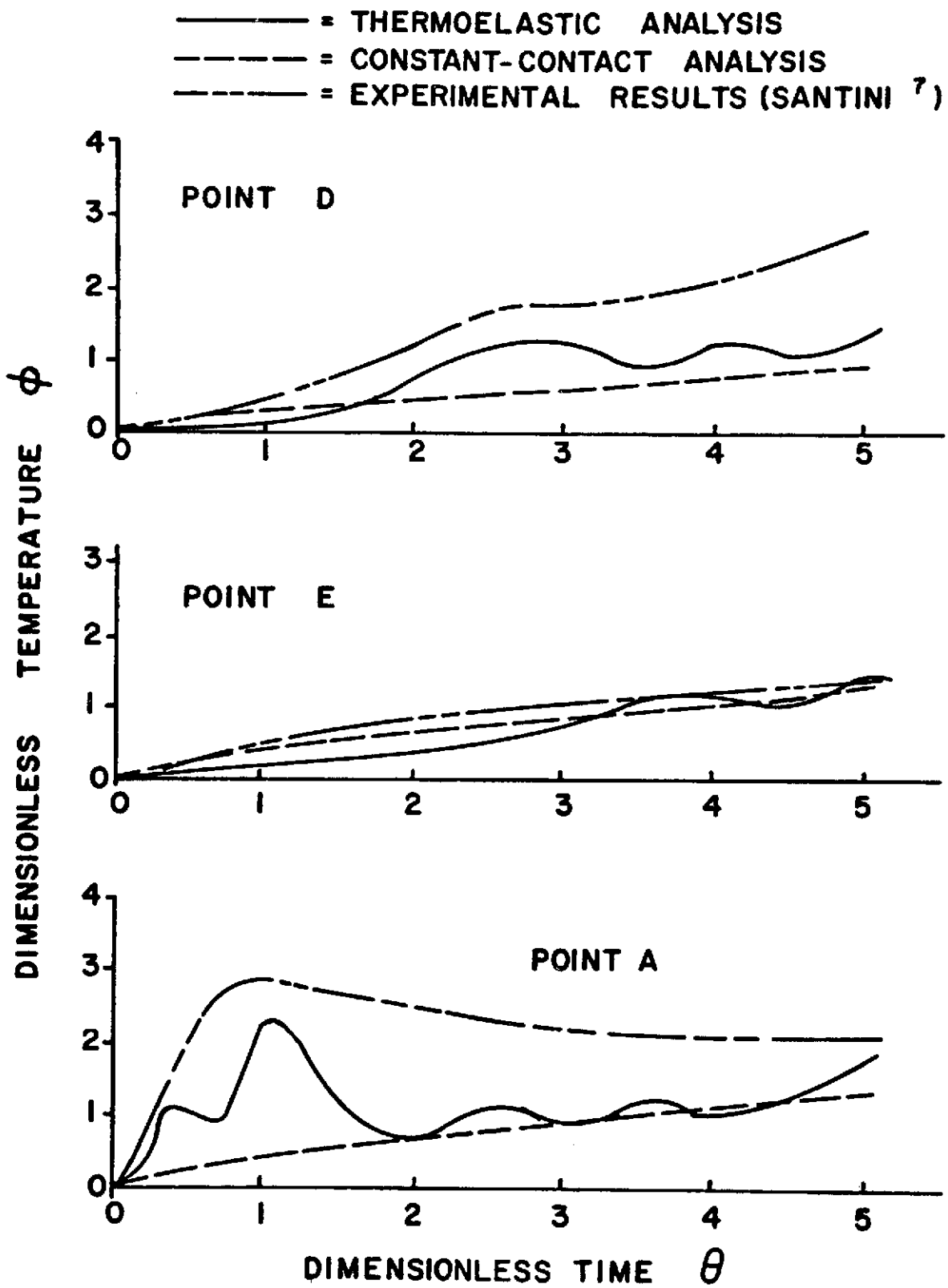

Figure 4. Transient Temperature Variation for Three Points on Contacting Surface of Single-Pad Brake

In reviewing all three sets of curves of Figure 4, it might be concluded that, although the thermoelastic analysis does not predict perfectly the magnitudes of the temperatures at points near the friction surface, it does give a better prediction than does the constant-pressure analysis used by investigators in the past. It is able to predict, with some degree of accuracy, the fluctuations in temperature caused by shifting of the contact areas.

It was mentioned earlier that the reason for the concentration of contact is thermal deformation of the contacting surfaces. Figure 5 shows this thermal deformation at $\theta = 0.75$ as determined by the thermoelastic analysis. The upper curve is for the top side of the strip of source elements at the contact surface while the lower curve is for the disk side of the elements. It can be seen that the greatest compressive deformation occurs near the elements that are in contact (see Fig.3).

Since we have calculated and noted the amount of wear that occurred in each worn element, we are able to determine a predicted wear rate for the single pad disk brake from our thermoelastic analysis. The wear rate determined in this manner is $.782 \times 10^{-8}$ m^3 of pad material/second, averaged out over the duration of the brake run, with the wear of disk material being negligible. Using the density of the pad material (4900 kg/m^3) and the initial pad mass (0.157 kg) we come up with an average ratio of mass of worn material/mass of original pad $\left(\frac{\Delta M}{M_o}\right)$ equal to .000244 kg/kg/second of run time. The experimentally determined value (Ref.7) is $\frac{\Delta M}{M_o}$ = .00019 kg/kg/sec of run time. Although our predicted value is about 28% higher than the actual value, it is felt that this difference is not at all bad considering the approximations used in determining the wear criterion, the discretization of the wear process, and the neglecting of plastic deformation prior to wear. Since the predicted wear rate is of the same order of magnitude as the actual, the assumed wear criterion must be quite reasonable.

4.2 Analysis of Annular Disk Brake

Having shown in the single-pad brake analysis that our method is reasonably valid, we will now turn our attention to a similar analysis of an aircraft disk brake having an annular stator. We will again use a finite element mesh similar to that shown in Figure 2 with the stator and rotor elements now both being

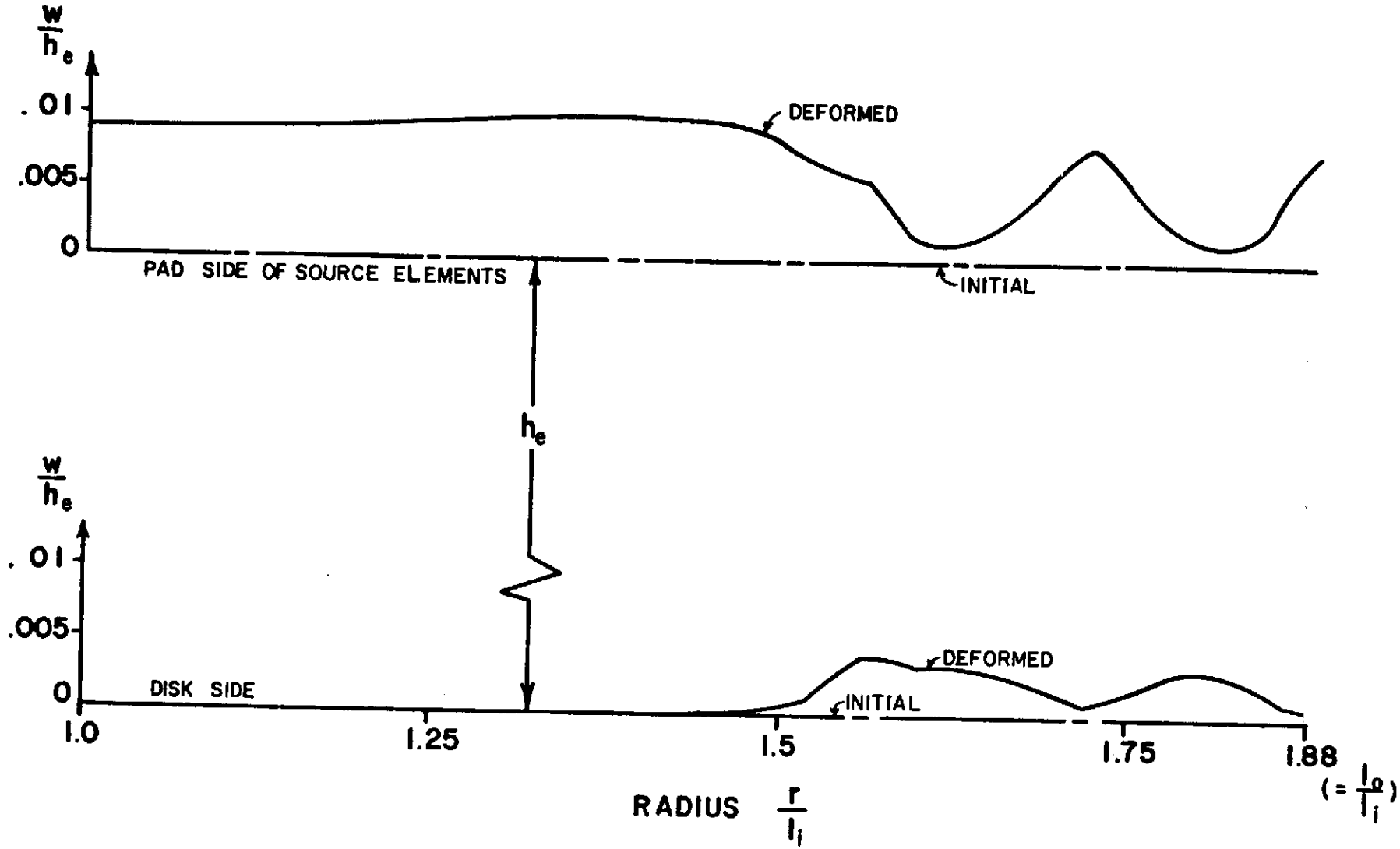

Figure 5. Thermal Deformation of Contacting Surfaces for Single-Pad Brake at $\theta = 0.75$. Top curves show initial and deformed configurations of stator pad side of friction surface source elements. Bottom curves show initial and deformed configurations of rotor disk side of elements.

complete rings. The geometry of the finite element idealization will be approximately that of a section of a brake from the Boeing 747 aircraft and the analysis will attempt to study the condition of rejected takeoff for that aircraft. In that condition the aircraft is braked from near-takeoff velocity to a complete stop in a very short time.

The material properties used will be those of the Boeing 747 brake materials. The only change in material from those used in the single-pad analysis will be the use of carbon steel for the stator backplate instead of aluminum. We will again have several elements of zero z-direction thermal conductivity at the interface where the friction pads are attached to the stator disk in order to account for thermal contact resistance there. All external surfaces are again assumed to be insulated for purposes of the analysis.

As with the single-pad analysis, the contact between friction pad and disk is assumed to be initially perfect, but immediately upon contact a non-uniform velocity distribution causes a larger heat generation rate near the outside radius of contact. This causes an immediate shift in contact toward the outside as can be seen in Figure 6. Because of the very high braking energies encountered in the rejected takeoff condition, temperatures increase rapidly inside the contact zone and wear begins to occur before the contact has had a chance to become concentrated. As Figure 6 shows, wear and shifting contact cause the contact zone to move away from the outside portion of the contact area much earlier than was observed in the single-pad analysis. Much more wear occurs in a shorter time than was seen in the single-pad study (Fig.3) and this causes more frequent shifts of contact area. It should be noted that, because of differences in brake radii, the dimensionless time grouping θa used in Figure 6 differs from the θ grouping used in Figure 3, with $\theta a = 1.0$ corresponding to $\theta = 0.338$.

The transient temperatures for various points inside the brake section are shown in Figure 7. Curves A are for point A, lying near the friction surface of the stator pad (see Fig.2). Point B lies on the center plane of the rotating disk at the same radius as point A and point C lies inside the friction pad at a point where the friction material meets the steel cup that encloses it. The solid curves of Figure 7 are for a variable contact analysis, while the dotted curves are for a constant contact analysis which neglects thermoelastic deformation. No published experimental data is available for comparison for the case of an annular brake. The dimensionless time τ for these curves equals t/t_f, where t_f is the elapsed braking time when the aircraft comes to a stop.

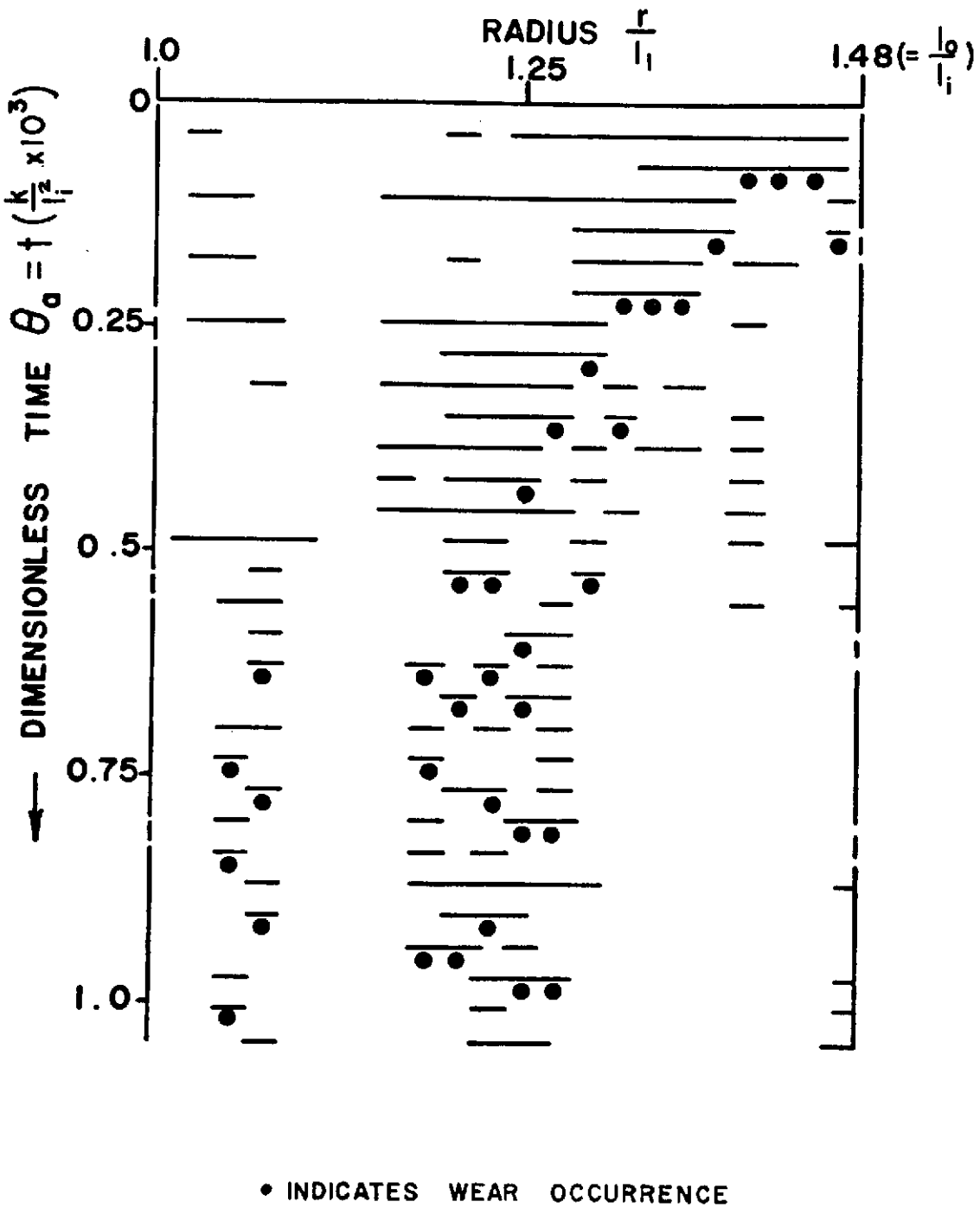

Figure 6. Transient Changes in Contact Area for Annular Disk Brake. Horizontal lines indicate portion of friction surface in instantaneous contact.

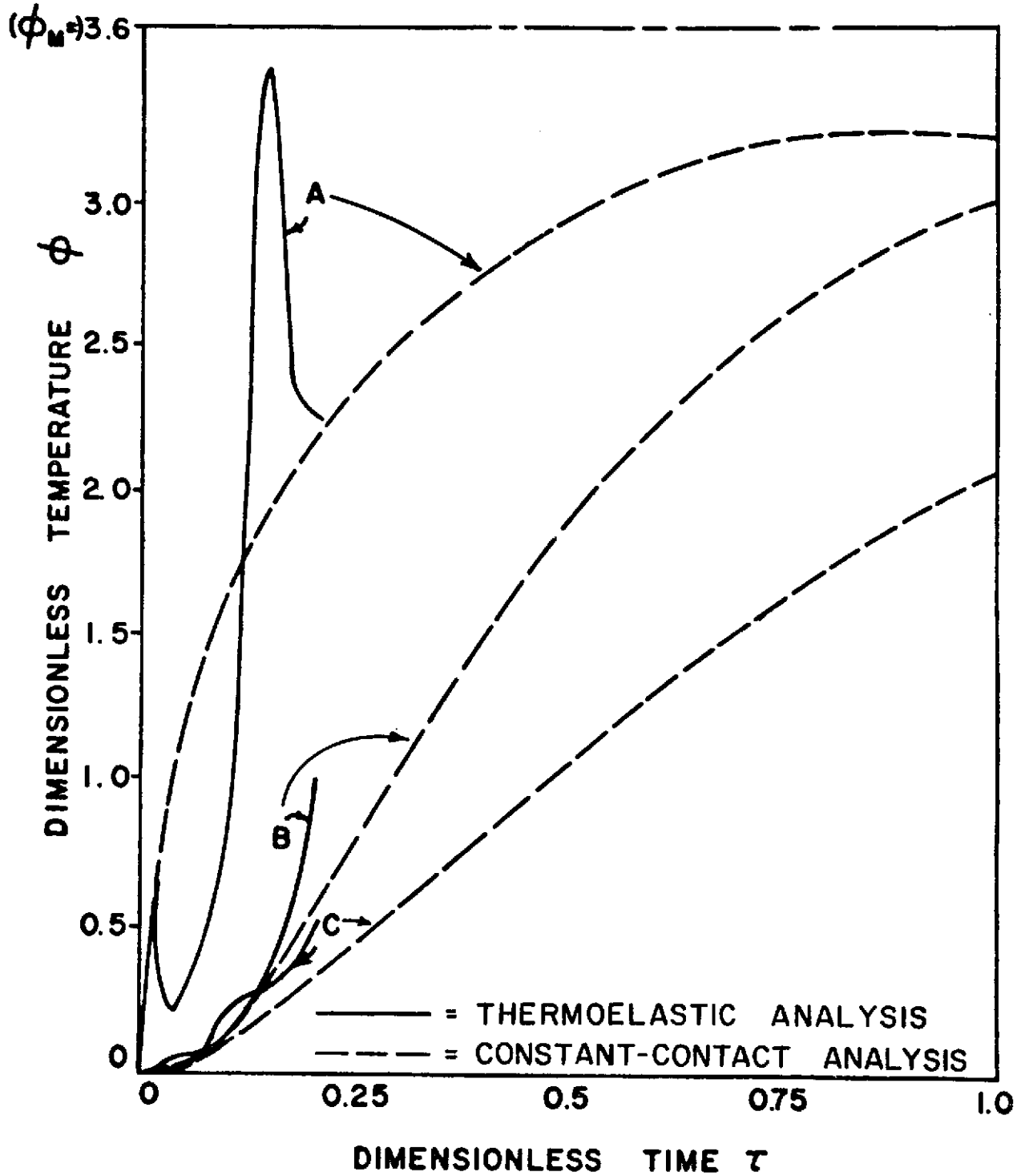

Figure 7. Transient Temperature Variation for Three Points in Annular Brake Assembly

It can easily be seen that the contact surface temperatures are higher than those inside either the pad or the disk. The temperatures calculated by the variable-contact analysis tend to be higher than those calculated by the constant-contact analysis, with relatively severe temperature fluctuations predicted near the contact surface by the thermoelastic analysis. The fluctuations are damped out considerably at points inside the brake components. The wide fluctuations near the contact surface are due to the very large heat energies that are generated in the concentrated contacts for this problem, but the ability of the contacting bodies to absorb and dissipate heat helps keep the temperatures inside the bodies from varying as rapidly. The temperatures have been found to be dependent on the material properties and geometry of the contacting components and these effects are examined more closely in the next sections.

The magnitudes of the temperatures attained in this problem are quite a bit larger than those found with the single-pad analysis because of the higher contact pressures in this rejected takeoff analysis. The melting temperature of the friction material is approximately $\varphi_m = 3.6$ and is shown on Figure 7. It can be seen that the temperatures at the concentrated contacts on the friction surface approach this temperature quite early in the braking cycle. This causes a problem with the thermoelastic analysis because of the very high wear rates at such high temperatures. We are faced with the choice of either making the time increments very small in order to decrease the amount of wear during each increment, or making a very large number of stress transfer iterations to complete the wear process if larger time increments are used. Either case requires a great deal of computer time and, because of this, the thermoelastic analysis had to be stopped early in the braking cycle.

It should be mentioned that when rejected takeoff conditions are encountered in practice the brakes face much the same conditions mentioned above, with very large amounts of wear and some melting occurring. Brakes that encounter such a service condition are replaced immediately, since they are no longer useable.

4.3 Effect of Thermal Parameters on Brake Temperatures

This part of the investigation is concerned with determining the effect of the different thermal properties of the disk brake materials on the temperature distribution in the brakes. In order to isolate the effect of the thermal parameters

under investigation, the effects of thermal deformation and wear were eliminated by setting the coefficient of thermal expansion (α) equal to zero for all materials in the brake, thus keeping the contact area constant. The configuration used in these tests was that shown in Figure 2, using a full-circle stator (annular friction pad).

It was desired to investigate the relative importance of the following thermal properties:

thermal conductivity of the disk (rotor) material)	k_{disk}
thermal conductivity of the friction pad material	k_{pad}
specific heat of the disk material	c_{disk}
specific heat of the friction pad material	c_{pad}

A series of five curves were obtained; one in which the properties of the conventional Boeing 747 brake materials were used, and four others, each having one thermal property differing from its original value. The changed values used in these four tests were not meant to correspond to those of any actual material, but were set at twice their normal values. The geometry was kept constant for all five tests.

The results of these tests are shown in Figures 8-10 for three different points inside the brake section. The reference values k_1 and $(\rho c)_1$ are, respectively, thermal conductivity and (density × specific heat) of the conventional friction pad material. The melting point of the conventional friction material, φ_m, is approximately 4.7 for the values of $\bar{\ell}$ and $\dot{Q}_o$ used in these computations.

Figure 8 shows the effect of the different thermal parameters on the temperature at the contact surface (pt. A in Fig.2). It can be seen that the maximum decrease in surface temperature is achieved when the heat capacity of the disk material is doubled (curve 5), with a doubling of the heat capacity of the pad (curve 3) being next most effective in reducing surface temperature. An increase in the thermal conductivity of the materials is not quite as effective in reducing contact surface temperatures (curves 2 and 4). The changes in conductivity caused significant reductions in surface temperature early in the braking cycle, but the magnitude of the reductions decreased later in the cycle. The temperature decrease resulting from increasing the specific heat, on the other hand, remained undiminished throughout the braking cycle.

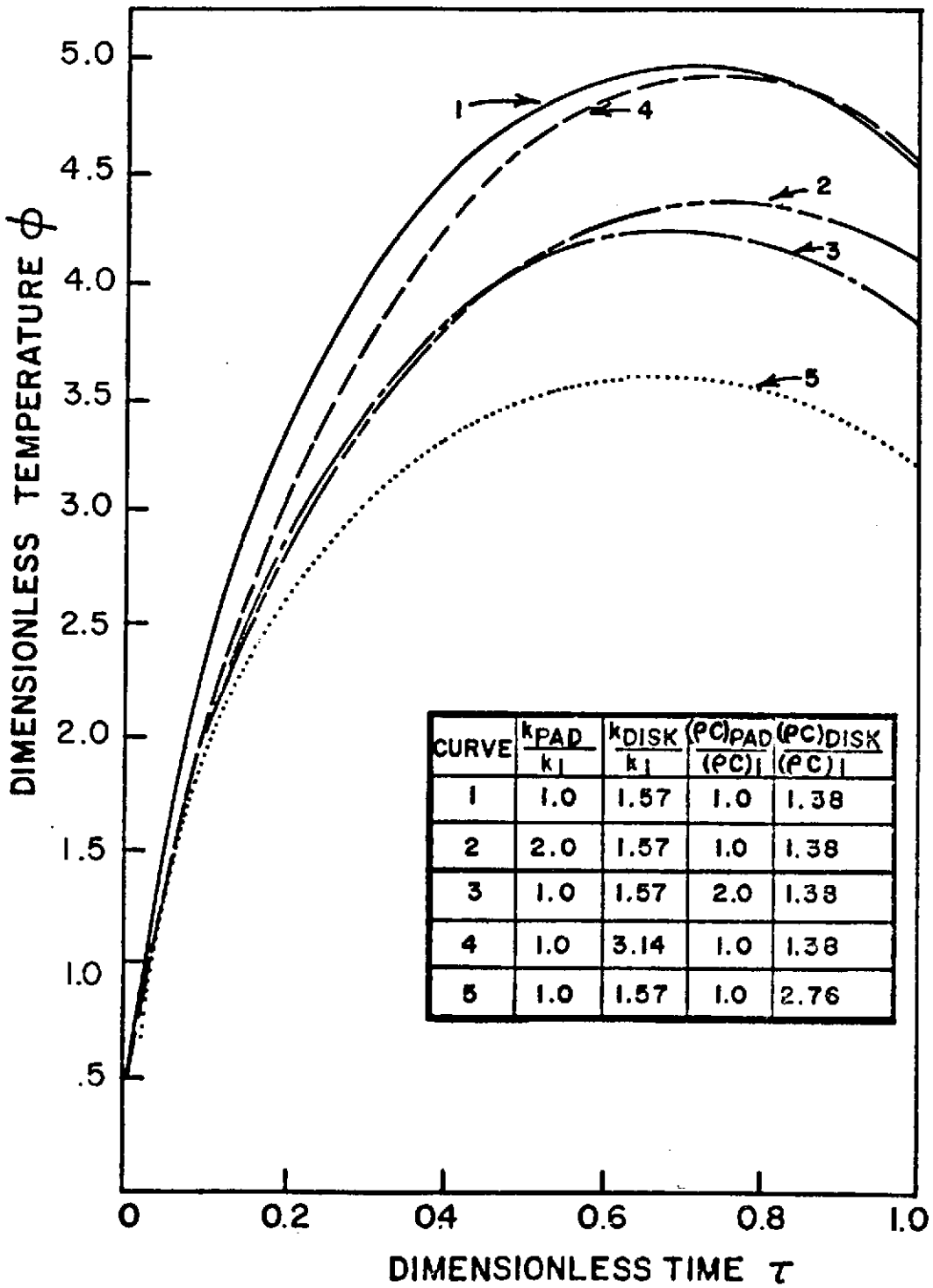

CURVE	$\frac{k_{PAD}}{k_1}$	$\frac{k_{DISK}}{k_1}$	$\frac{(\rho C)_{PAD}}{(\rho C)_1}$	$\frac{(\rho C)_{DISK}}{(\rho C)_1}$
1	1.0	1.57	1.0	1.38
2	2.0	1.57	1.0	1.38
3	1.0	1.57	2.0	1.38
4	1.0	3.14	1.0	1.38
5	1.0	1.57	1.0	2.76

Figure 8. Effect of Thermal Parameters on Transient Temperature at Point on Contact Surface

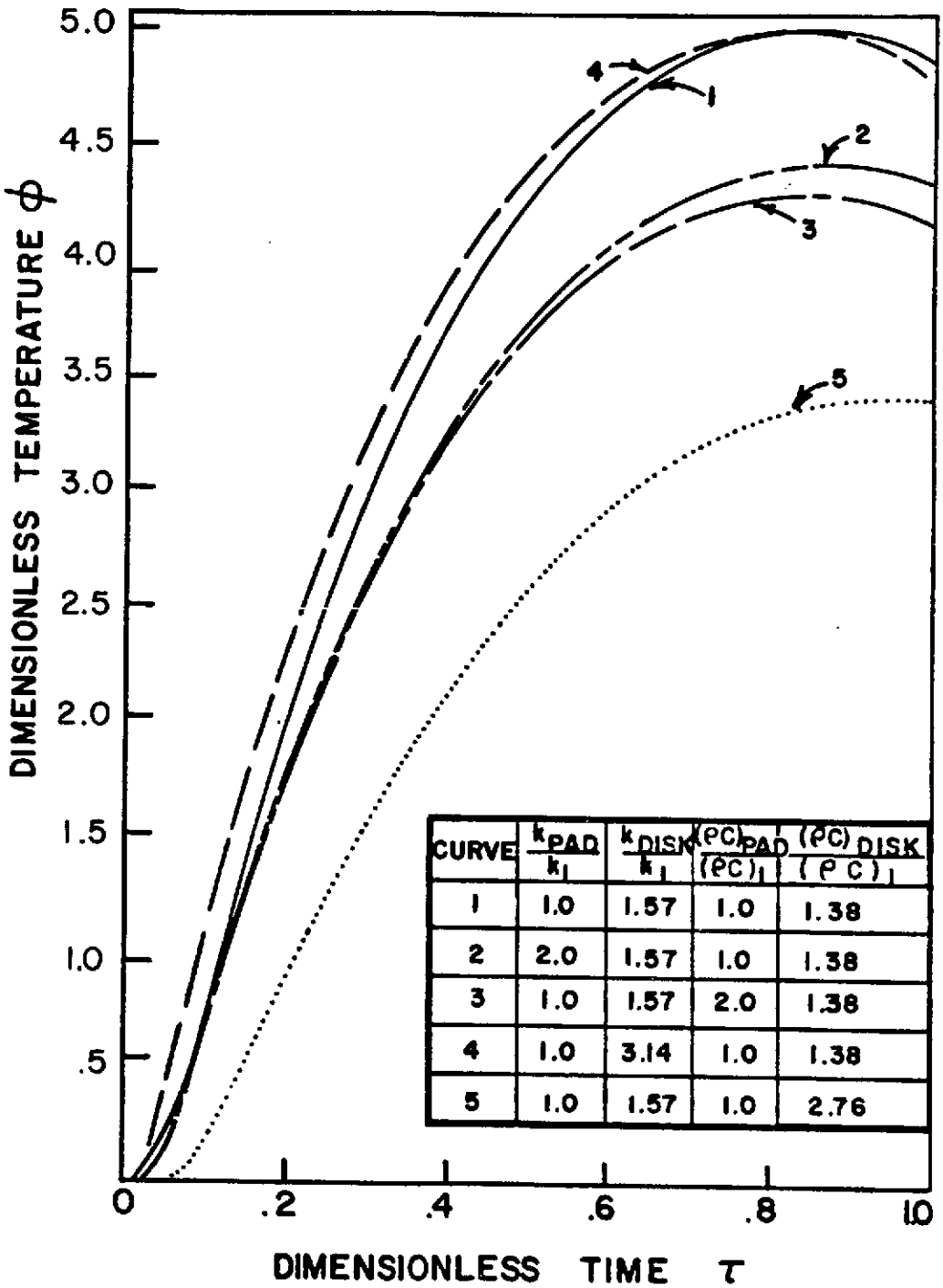

CURVE	$\frac{k_{PAD}}{k_1}$	$\frac{k_{DISK}}{k_1}$	$\frac{(\rho C)_{PAD}}{(\rho C)_1}$	$\frac{(\rho C)_{DISK}}{(\rho C)_1}$
1	1.0	1.57	1.0	1.38
2	2.0	1.57	1.0	1.38
3	1.0	1.57	2.0	1.38
4	1.0	3.14	1.0	1.38
5	1.0	1.57	1.0	2.76

Figure 9. Effect of Thermal Parameters on Transient Temperature at Point Inside Rotating Disk

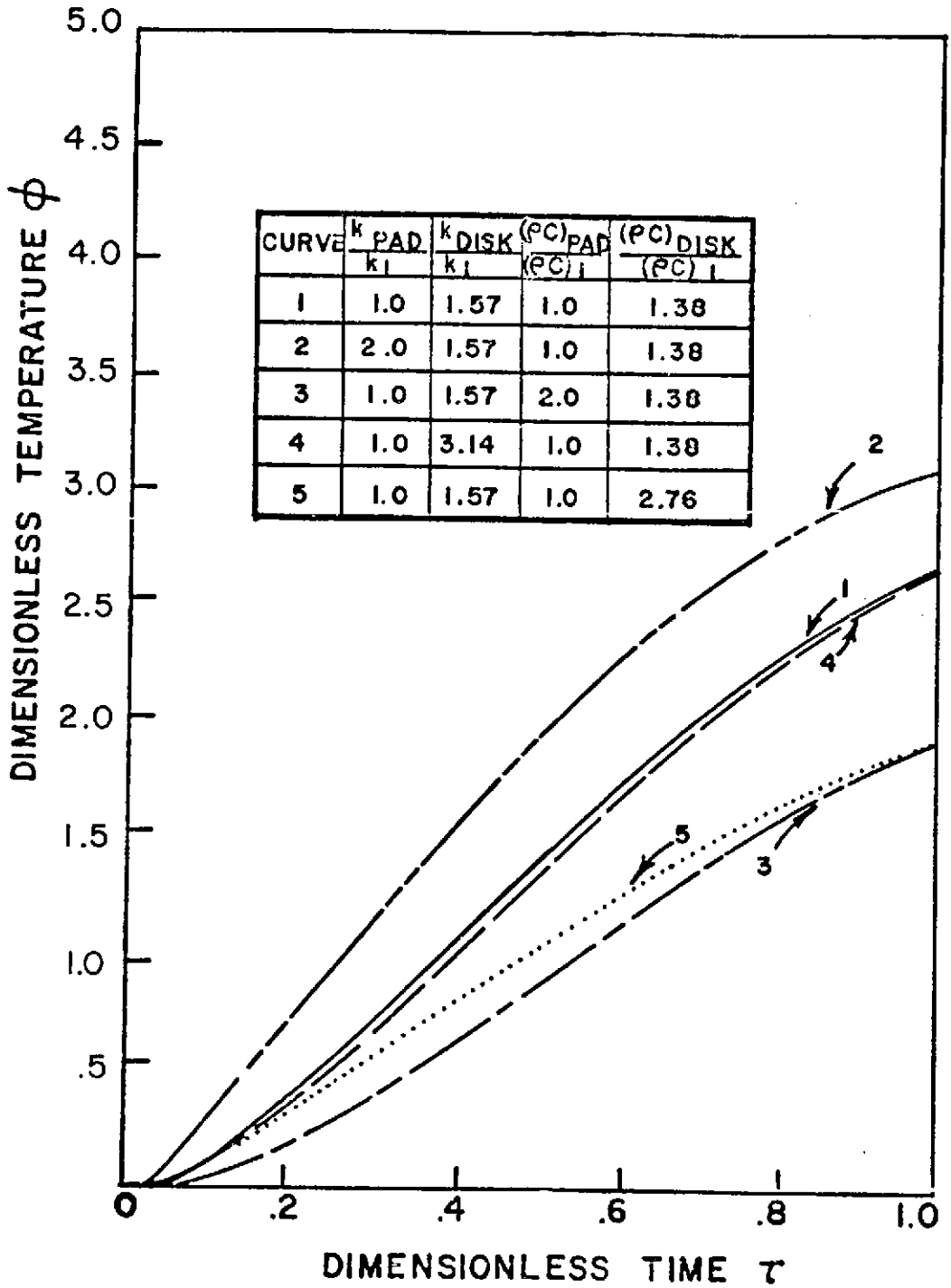

Figure 10. Effect of Thermal Parameters on Transient Temperature at Point Inside Friction Pad

The effects of the thermal property changes on the temperatures inside the rotating disk (point B in Fig.2) and inside the friction pad (pt. C) are shown in Figures 9 and 10, respectively. It can be seen that increasing the thermal conductivity of the disk material causes a temperature increase in the disk, at least through most of the braking cycle, while an increase in heat capacity of that material causes a decrease in temperature. The same effects on the temperature at a point inside the pad result from changing the pad material properties. The temperature at both points showed a decrease when either conductivity or specific heat of the opposite material was increased. As with the surface temperature, the greatest temperature decreases were brought about by a doubling of the heat capacity of the disk material with a doubling of the pad material heat capacity being next most effective.

As was mentioned earlier, the above results were found for fictitious combinations of material properties. Data for real materials yields similar results, however, as can be seen from Table 1. This set of tests, which was carried out to provide information for use in a brake material evaluation (Ref.22), shows the transient temperature variation at a point on the friction surface (pt. A in Fig.2) under rejected takeoff conditions. The contact area was again kept constant by setting $\alpha = 0$ in order to eliminate the effects of thermal deformation and wear.

The materials investigated are listed in Table 1 in order of increasing heat capacity (ρc). It can be seen that, in general, an increase in ρc leads to a decrease in surface temperature, as was found earlier from Figure 8. Although heat capacity seems to have a greater influence on surface temperatures, thermal conductivity is also important, as pointed out by the data for copper.

From our results it is apparent that the thermal properties of brake materials are very important if low brake temperatures are desired. The specific heat seems to be especially important since nearly all of the generated heat remains in the brake components during the short braking cycle and the components must, therefore, be able to absorb large quantities of heat without rising to excessive temperatures. The thermal conductivity is also important so that the generated heat can be conducted rapidly away from the friction surface.

The ideal brake material would have a high value for both ρc and k, and would also have a high melting temperature and exhibit all the other characteristics desirable for such applications (Ref.22). Such a material does not exist, however,

TABLE 1

TRANSIENT TEMPERATURE AT POINT A ON FRICTION SURFACE
FOR DIFFERENT FRICTION PAD MATERIALS

Friction Pad Material	$\frac{\rho c}{(\rho c)_1}$	$\frac{k}{k_1}$	Melting Point φ_m	Temperature φ at Point A		
				$\tau = \frac{1}{3}$	$\tau = \frac{2}{3}$	$\tau = 1$
Zirconium	.71	4.7	5.45	1.71	2.73	3.09
Conventional Friction Material	1.0	1.0	2.92	1.69	2.58	2.87
Molybdenum	1.15	7.5	7.65	1.47	2.33	2.64
Aluminum	1.18	11.8	1.98	1.42	2.26	2.55
Copper	1.35	21.0	3.2	1.33	2.09	2.38
Beryllium	1.37	7.8	3.78	1.35	2.14	2.43
Cobalt	1.44	3.7	4.41	1.34	2.14	2.42
Nickel	1.53	4.9	4.29	1.30	2.07	2.39
Cobalt-Base Superalloy	1.75	1.64	3.8	1.32	2.02	2.26

Notes:

1. For all cases, rotor material was medium-carbon alloy steel with $\frac{\rho c}{\rho c_1} = 1.38$ and $\frac{k}{k_1} = 2.43$.
2. Reference values are $k_1 = 18.84$ Joules/m sec^2K; $(\rho c)_1 = 2.57 \times 10^6$ Joules/$m^3{}^\circ K$.
3. Dimensionless variables are $\varphi = \frac{Tk_1\bar{\ell}}{\dot{Q}_o} \times 10^3$ and $\tau = t/t_f$.

and compromises must be made when choosing materials for brake applications. The results of this section indicate that when such a material is chosen, the thermal parameters should be optimized so that low surface temperatures will be produced.

The results of Figures 8-10 also seem to show that the amount of heat conducted away from the friction surface into a given material depends, not only on the conductivity of that material relative to the conductivity of the opposing material, but also on its relative ability to absorb heat (specific heat). Any partitioning of the generated heat must be a function of both thermal parameters.

4.4 Effect of Component Thickness on Brake Temperatures

In this section we will investigate the effect of the thickness of the brake components on the temperature distribution in an aircraft disk brake. We will again eliminate the effects of thermal deformation and wear by setting $\alpha = 0$ for all brake materials. Otherwise all material properties will be those of the conventional Boeing 747 brake materials and those properties will remain constant throughout the test series.

The temperature variation was plotted for the same three points considered in the previous section (one point inside friction pad, one point inside disk, one point on friction surface) and the results are shown in Figures 11-13. The pad thickness and disk half-thickness are given by H_{pad} and H_{disk}, respectively, with the thickness of a conventional Boeing 747 friction pad being H_1.

Figure 11 shows the effect of pad and disk thicknesses on the temperature at a point inside the pad. It is seen that a decrease in pad thickness results in a higher temperature at point C (curve 7) while an increase in thickness leads to a decrease in temperature (curve 6). This would be expected since the distance of point C from the friction surface changes as the pad thickness changes. In addition to these changes, it is also seen that variations in the thickness of the disk affect the temperature inside the friction pad, with an increase in the disk thickness causing a decrease in the temperature at point C (curves 8 and 9), and a decrease in disk thickness bringing about an increase in pad temperature (curve 10). This effect seems to indicate that the portion of the generated heat that enters the pad is affected by the volume of the disk.

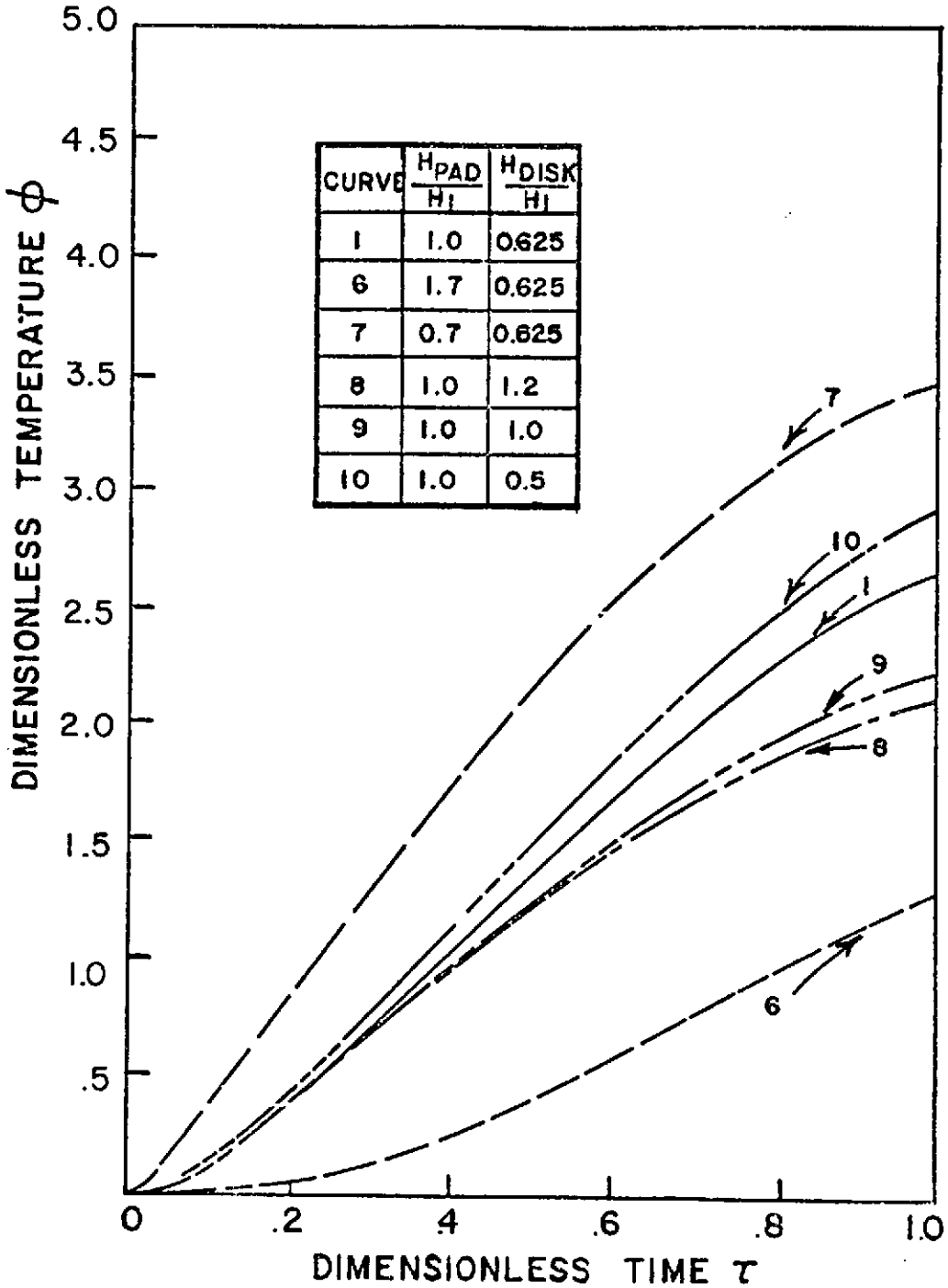

Figure 11. Effect of Geometrical Parameters on Transient Temperature at Point Inside Friction Pad

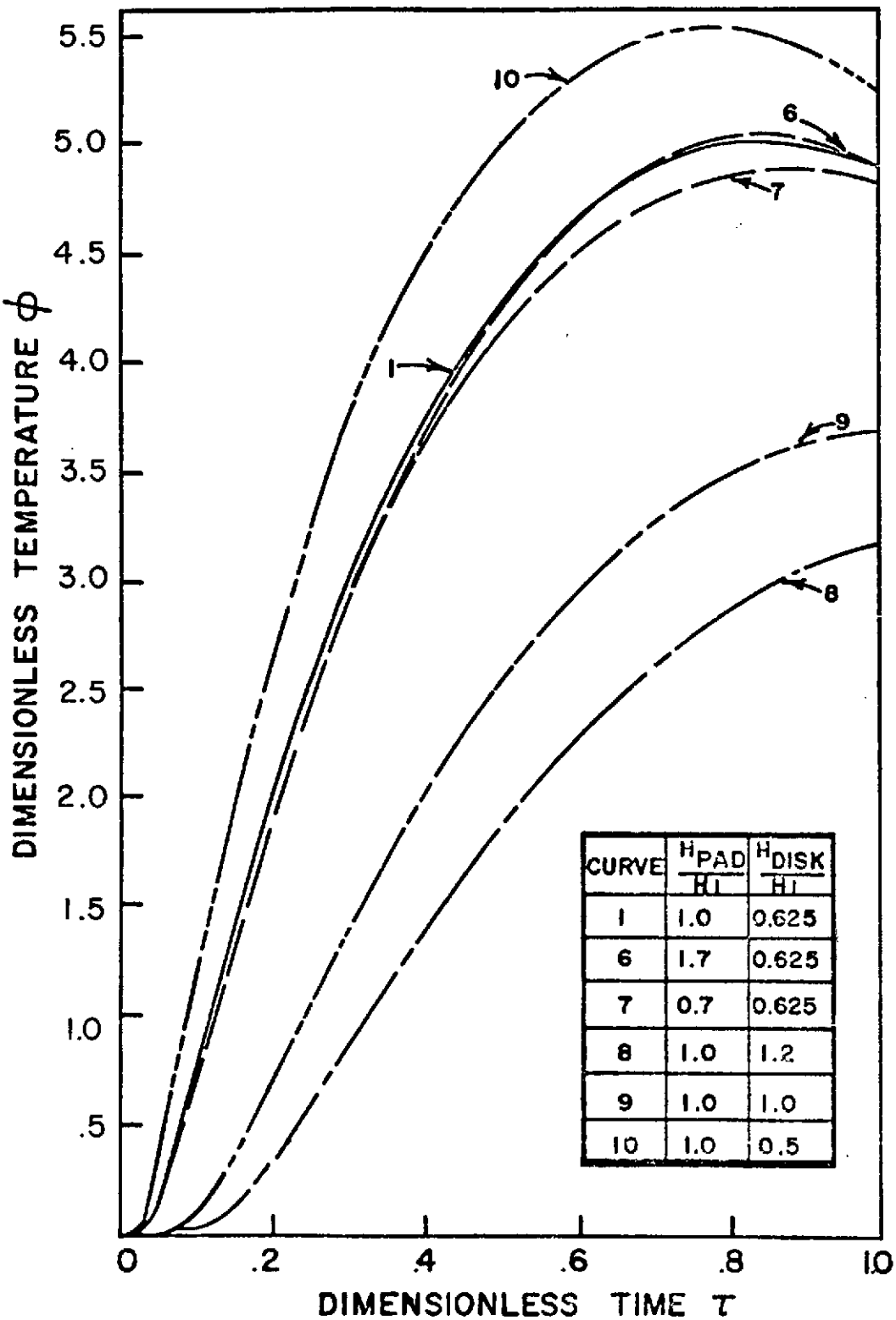

Figure 12. Effect of Geometrical Parameters on Transient Temperature at Point Inside Rotating Disk

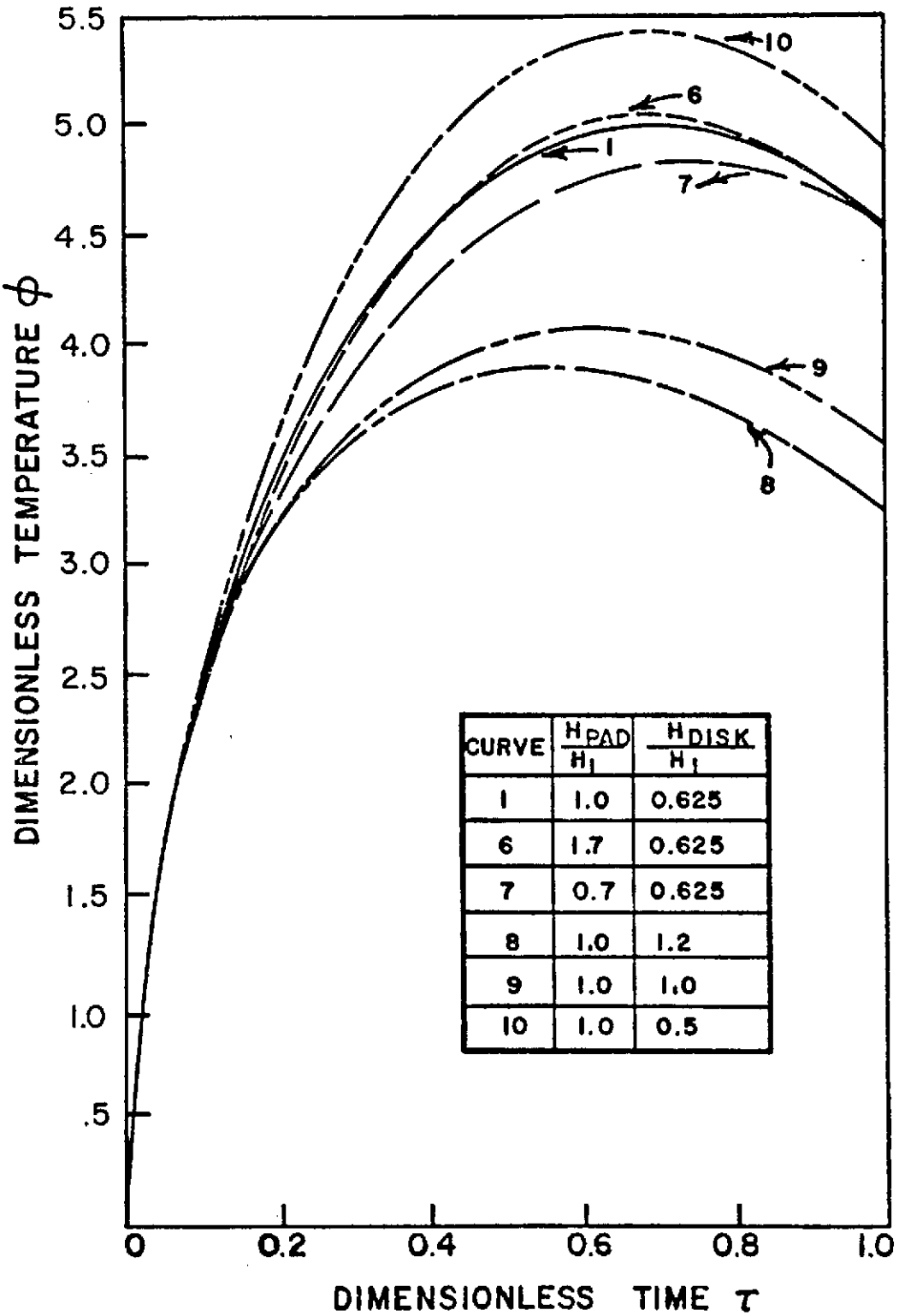

Figure 13. Effect of Geometrical Parameters on Transient Temperature at Point on Contact Surface

Looking next at Figures 12 and 13 one can see the effect of thickness on the temperature at point B inside the disk and at point A on the contacting surface. Curves 8, 9, and 10 produce results similar to those mentioned above, with an increase in disk thickness resulting in a lower temperature at both points B and A and a decrease in thickness resulting in a higher temperature. The magnitude of these changes is greater inside the disk (Fig.12) than on the contacting surface (Fig.13), as one might expect.

The effect of pad thickness on disk and surface temperatures seems to differ from our other results. As can be seen from curves 6 and 7, a decrease in pad thickness produces a slight decrease in temperature at both points B and A. The reason for this phenomenon seems to be that the friction pad under investigation consists of a friction material with rather low specific heat and conductivity, surrounded by a steel jacket with higher thermal properties. If the friction pad wears and the pad gets thinner, less low-conductivity friction material lies between the steel jacket and the friction surface, enabling the jacket to absorb more of the generated heat. This phenomenon is peculiar to configurations such as that investigated and would not be encountered in the case of a single-material stator.

From the above results one can see that the geometry of the brake components has a considerable effect on the temperature distribution in the brake. If low surface temperatures are desired, it would be advantageous to increase the volume of the heat sink, which in our case is the disk. It seems that by doing so, one increases the capacity of the heat sink to absorb heat and this allows more of the generated heat to flow into the sink material. Although there are exceptions, as with our pad configuration, it seems that the transient partitioning of generated heat is generally affected by the relative volumes of the contacting bodies, as well as by the thermal properties discussed in the previous section, and any partitioning relationship for sliding bodies of finite thickness should show this dependence.

SECTION 5

CONCLUSIONS

(1) The thermoelastic instabilities that cause changes in the areas of actual contact between sliding bodies can be modeled analytically by use of the finite element method. This process of contact area change can be briefly described as follows: Non-uniform thermal deformation of the contact surface causes concentration of contact at areas of largest deformation, resulting in higher temperatures being generated in those areas and more concentration of contact, until the stress level at the concentrated contact is so high that wear occurs and the contact shifts to another area, where the process repeats.

(2) Modeling of the wear process by using a wear criterion based on a critical, temperature-dependent distortion energy results in prediction of wear rates for a caliper disk brake that are the same order of magnitude as the wear rates determined experimentally.

(3) The transient temperature distribution in the components of a disk brake can be determined more accurately by use of this thermoelastic analysis than by an analysis that assumes constant contact conditions.

(4) The thermoelastic analysis described here is not as practical when the heat energy generated at the sliding surface is so high that near-melting-point temperatures and very high wear rates are produced at the concentrated contacts.

(5) The partitioning of the heat generated at the interface between two sliding bodies depends on the conductivity, density, specific heat, and volume of the two bodies.

(6) Lower temperatures in a disk brake assembly can be attained by increasing the conductivity, the volume and, especially, the heat capacity of the heat sink component. The development of new brake materials and improved component designs promises to be a major way to attain lower brake temperatures, which are very desirable from the standpoint of improved brake performance, decreased brake wear, and improved aircraft safety.

APPENDIX A

DEVELOPMENT OF FINITE ELEMENT EQUATIONS FOR THERMAL ANALYSES

If a body obeys Fourier's law of linear heat conduction, the heat equation in the body may be written in vector notation as:

$$\vec{\nabla} \cdot k \overrightarrow{\nabla T} + \dot{q} - \rho c \frac{\partial T}{\partial t} = 0 \qquad \text{(A1)}$$

where

T = temperature

k = thermal conductivity

ρ = density

c = specific heat

$\dot{q}$ = heat generation/unit volume.

The boundary of the body is considered to be composed of three regions, S_1, S_2, and S_3, with the following boundary conditions:

$$\begin{aligned} T &= T_c && \text{on } S_1 \\ \vec{q}^{o} \cdot \vec{n} &= k\overrightarrow{\nabla T} \cdot \vec{n} && \text{on } S_2 \\ -k\overrightarrow{\nabla T} \cdot \vec{n} &= h(T - T_a) && \text{on } S_3 \end{aligned} \qquad \text{(A2)}$$

where

T_c = prescribed temperature

$\vec{q}^{o}$ = prescribed heat flux

$\vec{n}$ = normal vector to surface

h = convection coefficient

T_a = ambient temperature.

It can be shown (Ref.13) that the solution of Eq.(A1) with the boundary conditions (A2) is equivalent to finding a stationary value of a functional I with respect to admissible variations in T, where

$$I = \int_V \left[\left(\rho c \frac{\partial T}{\partial t} - \dot{q}\right)T + \frac{k}{2}\left(\overrightarrow{\nabla T} \cdot \overrightarrow{\nabla T}\right)\right] dV + \int_{S_2} (-\vec{q}^{o} \cdot \vec{n})T \, dA + \int_{S_3} \frac{h}{2}(T - T_a)^2 \, dA \qquad \text{(A3)}$$

subject to the condition $T = T_c$ on S_1.

If the body (or system) under investigation is composed of N finite elements, then for the body we have:

$$I = \sum_{i=1}^{N} I^{e_i}$$

and our variational principle is

$$\delta I = \sum_{i=1}^{N} \delta I^{e_i} = 0 \tag{A4}$$

for admissible variations in T.

We will now form the variation δI^e for a ring element of triangular cross section for use in an axisymmetric thermal analysis. For such an element we assume a linear temperature distribution in the element of the form:

$$T = T_1 L_1 + T_2 L_2 + T_3 L_3 = \{L^e\}^T \begin{Bmatrix} T_1 \\ T_2 \\ T_3 \end{Bmatrix}^e \tag{A5}$$

where 1,2,3 are the nodes of the element and the T_i are the temperatures at those nodes.

It can be easily shown, using area coordinates, that the shape functions L_i^e, for the element are given by:

$$L_i^e = \frac{1}{2A}\left[(r_j z_k - r_k z_j) + r(z_j - z_k) + z(r_k - r_j)\right] = \frac{1}{2A}\left[a_i + b_i r + d_i z\right] \tag{A6}$$

where A is the cross-sectional area of the triangular element, and i, j, k = = 1, 2, 3 (cyclic permutation).

If we write the vector quantities in (A3) in cylindrical coordinates, allow the material to have transversely isotropic heat conduction properties ($k_r \neq k_z$), and use (A5) and (A6), we find that the first variation of I for a triangular ring element is given by

$$\delta I^e = \left[\int_V \left(\left(\rho c \frac{\partial T}{\partial t} - \dot{q}\right)\{L^e\}^T + \frac{1}{4A^2}\left([B] + [C]\right)\right)\begin{Bmatrix} T_1 \\ T_2 \\ T_3 \end{Bmatrix} dV - \int_{S_2} (\vec{q}^o \cdot \vec{n})\{L^e\}^T dA \right.$$

$$\left. + \int_{S_3} h\left(\{L^e\}^T \begin{Bmatrix} T_1 \\ T_2 \\ T_3 \end{Bmatrix} - T_a\right)\{L^e\}^T dA\right] \begin{Bmatrix} \delta T_1 \\ \delta T_2 \\ \delta T_3 \end{Bmatrix}^e \tag{A7}$$

where $B_{ij} = k_r b_i b_j$ and $C_{ij} = k_z d_i d_j$.

In order to take care of the time dimension, let us divide the total time interval of interest into small time increments and proceed in a step-by-step procedure. We will assume that the time increments are small enough so that the variation of temperature with time during the increment may be approximated by

$$T_t = T_{t-\Delta t} + \left(\left.\frac{\partial T}{\partial t}\right|_{t-\Delta t} + \left.\frac{\partial T}{\partial t}\right|_{t}\right)\frac{\Delta t}{2} \tag{A8}$$

We now sum the δI^e given in (A7) over all elements and apply the variational principle (A4) at both the beginning of the increment ($t-\Delta t$) and the end of the increment (t). Using (A8) we get the following expression for the set of nodal temperatures T_i at the end of the increment that satisfy our field equation (A1) with boundary conditions (A2)

$$\left([G] + \frac{2}{\Delta t}[R]\right)\{T_i\}_t = \left(\frac{2}{\Delta t}[R] - [G]\right)\{T_i\}_{t-\Delta t} - \{F\}_t - \{F\}_{t-\Delta t} \tag{A9}$$

where

$$G_{ij} = \sum_{k=1}^{N}\left(h\int_{S_3} L_i L_j\, dA + \frac{1}{4A^2}\left[k_r b_i b_j + k_z d_i d_j\right]\int_V dV\right)_{e_k}$$

$$F_i = \sum_{k=1}^{N}\left(-\dot{q}\int_V L_i\, dV - hT_a\int_{S_3} L_i\, dA - \vec{q}^{\,o}\cdot\vec{n}\int_{S_2} L_i\, dA\right)_{e_k}$$

$$R_{ij} = \sum_{k=1}^{N}\left(\rho c\int_V L_i L_j\, dV\right)_{e_k} \qquad \{T_i\} = \sum_{k=1}^{N}\left\{\begin{matrix}T_1\\T_2\\T_3\end{matrix}\right\}^{e_k}.$$

Defining:

$$[TS] \equiv [G] + \frac{2}{\Delta t}[R]$$

and

$$\{FT\} \equiv \left(\frac{2}{\Delta t}[R] - [G]\right)\{T_i\}_{t-\Delta t} - \{F\}_t - \{F\}_{t-\Delta t}$$

we may write (A9) as

$$[TS]\{T_i\}_t = \{FT\}. \tag{A10}$$

APPENDIX B

FLOW CHART FOR SOLUTION OF SLIDING-CONTACT PROBLEM

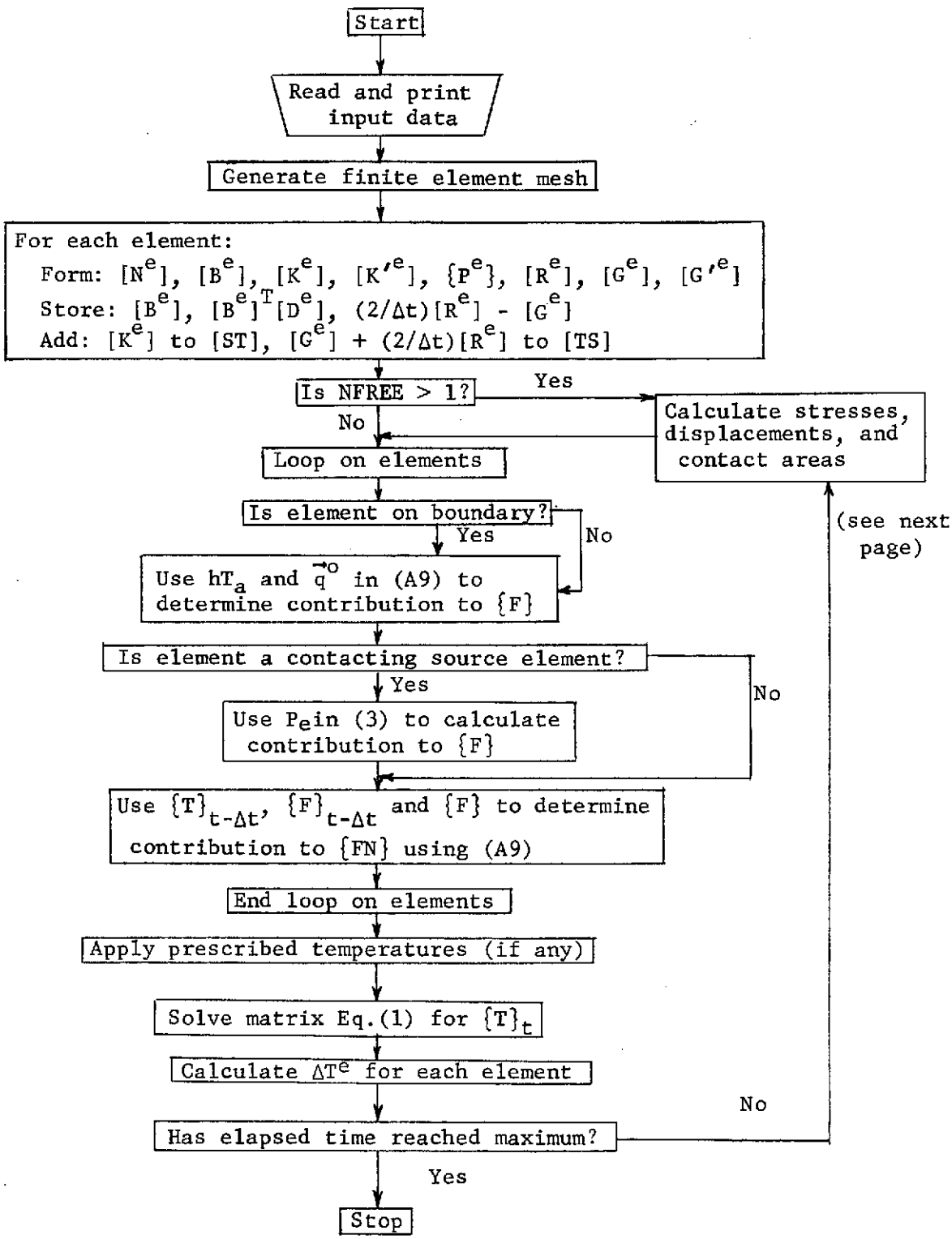

Calculation of Stresses, Displacements, and Contact Areas

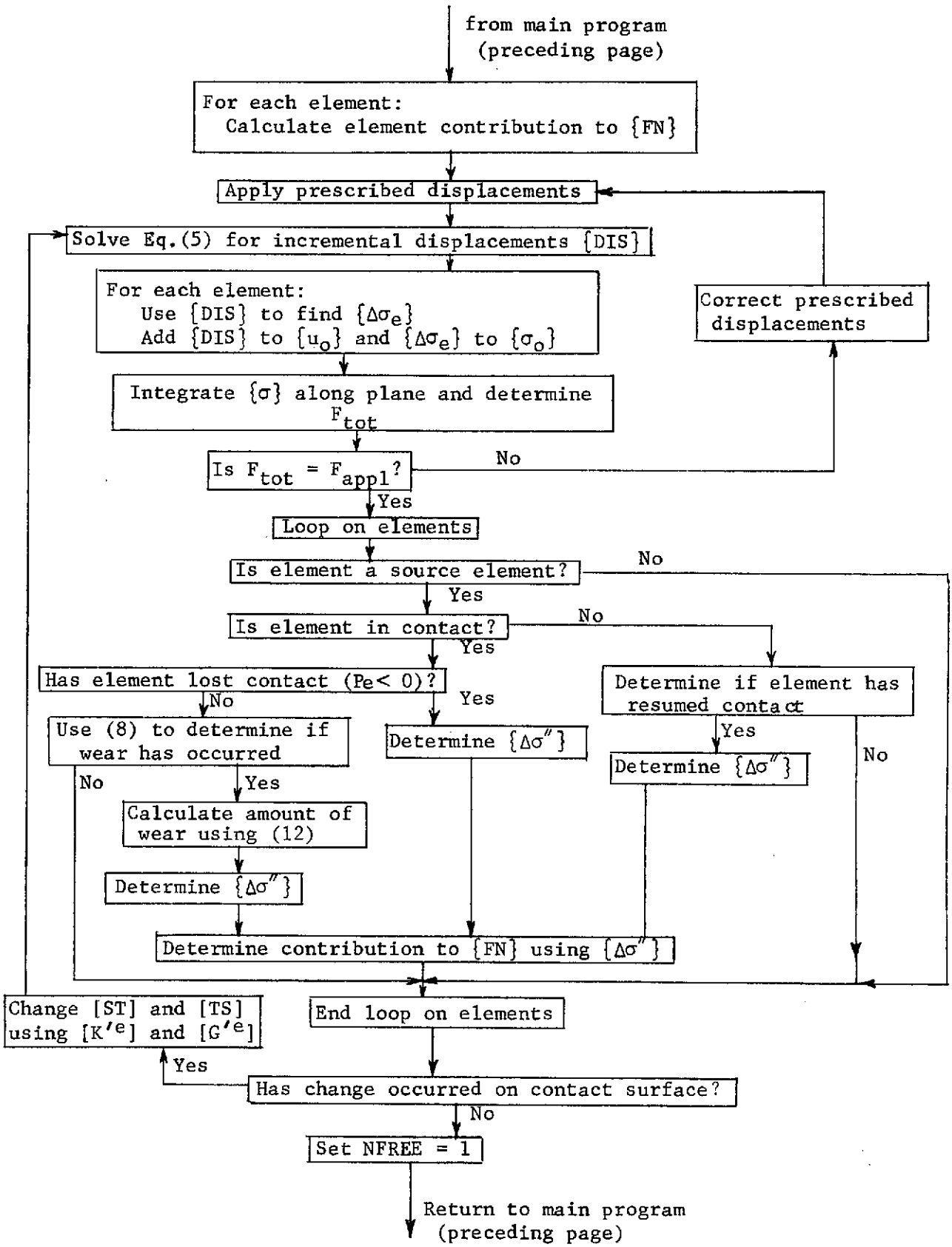

NOMENCLATURE

a_i - geometric constants used in shape functions [Eq.(A6)]

b_i - geometric constants used in shape functions [Eq.(A6)]

c - specific heat

c_1 - reference value of specific heat

d_i - geometric constants used in shape function [Eq.(A6)]

f - coefficient of friction

h_e - thickness of source element

h - film heat transfer coefficient (convection)

k - thermal conductivity

k_1 - reference value of thermal conductivity

$\bar{\ell}$ - average radius of friction surface

ℓ_i - inside radius of friction surface

ℓ_o - outside radius of friction surface

$\vec{n}$ - outer normal vector to boundary surface

$\dot{q}$ - heat generation rate/unit volume

$\vec{q}^o$ - prescribed heat flux

r_o - outside radius of element

r_i - inside radius of element

$\bar{r}$ - centroidal radius of element

t - time (measured from beginning of braking)

Δt - length of time increment

t_f - elapsed braking time when aircraft comes to stop

$\{u_o\}$ - matrix of nodal displacements before increment

w - displacement in z-direction

w_w - thickness of worn material from one wear occurrence

A - cross-sectional area of triangular finite element

A_p - contacting area of stator source element

A_D - contacting area of rotor source element

$[B]$ - matrix defined in Eq.(A7)

$[C]$ - matrix defined in Eq.(A7)

$[D]$ - constitutive relationship matrix for elastic elements [Eq.(7)]

$[D']$ - constitutive relationship matrix for fissured elements [Eq.(6)]

$\{DIS\}$ - matrix of incremental nodal displacements

E - modulus of elasticity

$\{F\}$ - matrix defined in Eq.(A9)

$\{FT\}$ - matrix of thermal loads [Eq.(A10)]

$\{FN\}$ - matrix of nodal loads

$\{F_T\}$ - matrix of nodal thermal stress loads

$\{F_F\}$ - matrix of nodal body force loads

$\{F_S\}$ - matrix of nodal surface traction loads

F_{appl} - force applied to brake by hydraulic pistons

F_{tot} - resultant force acting on friction surface

$[G]$ - matrix defined in Eq.(A9)

H_{pad} - thickness of stator friction pad

H_{disk} - half-thickness of rotor disk

H_1 - reference value of stator pad thickness

I - functional in variational principle for thermal analysis

J - mechanical equivalent of heat

J_2 - second invariant of stress deviator tensor

$[K^e]$ - element stiffness matrix

$\{L\}$ - matrix of shape functions

ΔM - mass of worn material

M_o - original mass

N - number of finite elements in domain

P_e - pressure acting normal to friction surface in source element

$\{P\}$ - matrix of concentrated nodal forces

$\{P''\}$ - matrix of nodal forces used in stress transfer process

$\dot{Q}$ - heat generation rate

$\dot{Q}_o$ - initial rate of heat generation

$[R]$ - matrix defined in Eq.(A9)

$[ST]$ - system stiffness matrix

$[TS]$ - thermal "stiffness" matrix [Eq.(A10)]

T - temperature (uniform initial temperature $\equiv 0$)

$\{T_i\}$ - matrix of nodal temperatures

T_a - ambient temperature

T_c - prescribed temperature

V - volume of finite element

W - critical value of J_2 for wear to occur

α - coefficient of thermal expansion

β - included angle of ring sector

δ - displacement of midplane A-A

$\{\epsilon\}$ - elastic strain matrix for element

$\{\epsilon_w\}$ - strain occurring in element during wear

θ - dimensionless time $\equiv t\left(\frac{k}{\ell_i^2} \times 10^3\right)$

θ_a - dimensionless time for annular analysis

ν - Poisson's ratio

π^e - potential energy functional for element

ρ - density

$(\rho c)_1$ - reference value of density × specific heat

$\{\sigma\}$ - stress matrix for element

$\{\sigma_e\}$ - elastic stress matrix for element

$\{\sigma'\}$ - stress in element after wear or fissuring

$\{\Delta\sigma''\}$ - stress to be transferred from worn or fissured element

$\{\sigma_o\}$ - stress in element before wear

$\{\sigma_w\}$ - stress relieved in element by one wear occurrence

σ_y - yield stress

σ_{zz} - z-component of stress in element if no wear had occurred

τ - dimensionless time $\equiv t/t_f$

$\tau_{rz}, \tau_{z\theta}$ - shear stress components

φ - dimensionless temperature $\equiv \dfrac{T\, k_1 \bar{\ell}}{\dot{Q}_o} \times 10^3$

φ_m - dimensionless melting temperature

$\dot{\omega}$ - angular deceleration of wheel

Ω - initial angular velocity of wheel

Subscripts not defined above

r,θ,z - cylindrical coordinates

i - node number

Superscripts

e - refers to one element

REFERENCES

1. Blok, H., "Theoretical Study of Temperature Rise at Surfaces of Actual Contact under Oiliness Lubricating Conditions," Proc. Gen. Discussion on Lubrication, Inst. Mech. Engrs., London, Vol.2, pp.222-235, 1937.
2. Jaeger, J.C., "Moving Sources of Heat and the Temperature at Sliding Contacts," Proc. of the Roy. Soc. of New South Wales, Vol.76, pp.203-224, 1942.
3. Ling, F.F. and Pu, S.L., "Probable Interface Temperatures of Solids in Sliding Contact," Wear, Vol.7, No.1, pp.23-34, 1964.
4. Ling, F.F., "On Temperature Transients at Sliding Interface," Trans. ASME, J. Lub. Tech., Series F, Vol.91, pp.397-405, 1969.
5. Parker, R.C. and Marshall, P.R., "The Measurement of the Temperature of Sliding Surfaces with Particular Reference to Railway Brake Shoes," Proc. Inst. of Mech. Engrs., Vol.158, pp.209-229, 1948.
6. Barber, J.R., "Thermoelastic Instabilities in the Sliding of Conforming Solids," Proc. Roy. Soc., A, Vol.312, pp.381-394, 1969.
7. Santini, J.J., "Effect of Design Factors on the Generation of Surface Temperatures in a Sliding System," D. Eng.Dissertation, Rensselaer Polytechnic Institute, June 1973.
8. Korovchinski, M.V., "Plane-Contact Problem of Thermoelasticity during Quasi-Stationary Heat Generation on the Contact Surfaces," Trans. ASME, J. Basic Eng., Series D, Vol.87, pp.811-817, 1965.
9. Dow, T.A. and Burton, R.A., "Thermoelastic Instability of Sliding Contact in the Absence of Wear," Wear, Vol.19, pp.315-328, 1972.
10. Newcomb, T.P., "Temperatures Reached in Disk Brakes," J. Mech. Eng. Sci., Vol.2, No.3, pp.167-177, 1960.
11. Fazekas, G.A.G., "Temperature Gradients and Heat Stresses in Brake Drums," SAE Trans., Vol.61, pp.279-308, 1953.
12. Chichinadze, A.V., "Temperature Distribution in Disk Brakes," Friction and Wear in Machinery, Trans. ASME, Vol.15, pp.259-275, 1962.
13. Visser, W., "A Finite Element Method for the Determination of Non-Stationary Temperature Distribution and Thermal Deformations," Proc. of the First Conference on Matrix Methods in Structural Analysis, Wright-Patterson AFB, Ohio, pp.925-928, 1965.
14. Zienkiewicz, O.C., The Finite Element Method in Engineering Science, McGraw-Hill Publishing Co. Ltd., 1971.

15. Kennedy, F.E., "Analysis of Nonlinear Contact Problems by the Finite Element Method," Ph.D. Dissertation, Rensselaer Polytechnic Institute, 1972.
16. Zienkiewicz, O.C., Valliappan, S., and King, I.P., "Stress Analysis of Rock as a 'No Tension' Material," Geotechnique, Vol.18, pp.56-66, 1968.
17. Kragelskii, I.V., Friction and Wear, Butterworths, Inc., 1965.
18. Rabinowicz, E., Friction and Wear of Materials, John Wiley & Sons, Inc., 1965.
19. Archard, J.F., "Wear," in Proc. of Interdisciplinary Approach to Friction and Wear, NASA, 1968.
20. Lancaster, J.K., "The Influence of Temperature on Metallic Wear," Proc. Phys. Soc. of London, B 70, pp.112-118, 1957.
21. Mac Gregor, C.W., ed., Handbook of Analytical Design for Wear, Plenum Press, 1964.
22. Peterson, M.B. and Ho, T.L., "Consideration of Materials for Aircraft Brakes," NASA CR-121116, April 1972.